J. Fluid Mech. (1990), *vol.* 214, *pp.* 131–159
Printed in Great Britain

Free–forced interactions in developing meanders and suppression of free bars

By M. TUBINO AND G. SEMINARA
Istituto di Idraulica, Università di Genova, Italy

(Received 9 September 1988 and in revised form 18 May 1989)

The coexistence of migrating alternate (free) bars, spontaneously developing in erodible channels as a result of an instability process, with steady point bars, forced by curvature in meandering reaches of rivers, is investigated theoretically.

A perturbation expansion is set up in terms of two dimensionless small parameters, ϵ and ν respectively, describing free and forced perturbations. The effect of mixed interactions at $O(\nu^2\epsilon^{\frac{1}{2}})$ is found to be responsible for the damping and slowing down of free bars as channel curvature increases. The theory allows us to determine the threshold value of channel curvature above which free bars are suppressed as a function of meander wavenumber for given flow and sediment characteristics. The minimum channel sinuosity for free bar suppression is found to be associated with the resonant wavenumber range of Blondeaux & Seminara (1985). Theoretical predictions compare satisfactorily with experimental observations by Kinoshita & Miwa (1974). The theory also suggests that free bars may appear again in a more advanced stage of meander development in accordance with field observations by Kinoshita (1961).

1. Introduction

Under widely occurring circumstances flow in a straight channel with erodible bottom is unstable and large-scale migrating bedforms develop which are characterized by a sequence of steep consecutive diagonal fronts with deep pools at the downstream face and gentler riffles along the upstream face. These bedforms which are often displayed by straight reaches of rivers at very low stage are known in the literature as 'alternate bars' and will be called 'free bars' in the following in order to emphasize the spontaneous character of their development. The formation of free bars in straight channels was the subject of several investigations developed mainly in the seventies (see Colombini, Seminara & Tubino (1987) hereinafter referred to as CST). Besides the practical importance of the subject (the presence of free bars affects several aspects of fluvial engineering like navigation, bank protection, design of fluvial structures), motivation for the above studies came from the idea that free bars, giving rise to a sinuous migrating thalweg within the initially straight banks, might somehow evolve into meanders provided channel banks be also erodible. In other words the formation of alternate bars (bar instability) would imply incipient meandering.

A different point of view was taken in the early eighties by Ikeda, Parker & Sawai (1981) who investigated the occurrence of a different type of instability, thereafter called 'bend instability', whereby planimetric perturbations of the channel axis may be destabilizing through the effect of bank erosion associated with secondary flow

induced by the formation of 'forced bars' due to a channel sinuosity, however small. The 'bend' mechanism was found to exhibit maximum growth for values of the meander wavelength close to those characteristic of alternate bars, thus supporting the, as yet, vague idea that the formation of alternate bars might proceed into a planimetric instability leading to the development of a meandering channel with initial wavelength close to that of alternate free bars.

Various questions arise from the new perspective opened up by the latter important contribution. What is the relationship between 'bar' and 'bend' instabilities? Since the timescale of the 'bend' process is that of bank erodibility the latter process appears to be very slow compared with the development of free bars in the initially straight channel. Thus the 'bend' mechanism is likely to operate in a channel where free bars have already developed. What is then the influence of the previously formed free bars on the bend instability process? In other words how do migrating free bars, spontaneously developing, affect steady bars forced by curvature?

The former question was tackled by Blondeaux & Seminara (1985) (hereinafter referred to as BS) by means of a unified approach to bar–bend instability somewhat modified with respect to that of Ikeda *et al.* (1981). It turned out that forced perturbations selected by the 'bend' mechanism coincide with free perturbations characterized by nearly vanishing complex growth rate. In other words the bend process is essentially a quasi-resonance phenomenon triggered by channel sinuosity.

The latter question is strongly related to its dual counterpart: how do forced bars induced by channel curvature affect free bars? This problem, namely the coexistence of free and forced bars, was experimentally investigated by Kinoshita & Miwa (1974) in an interesting paper (hereinafter referred to as KM) published in Japanese which remained unknown to us until recently when Professor Parker kindly provided us with a copy of an English translation of it.

KM investigated the behaviour of free bars in a meandering channel formed 'from straight segments at an angle α to each other' such that the resulting wavelength was either equal to, or a fraction of, the free bars which had been previously found to form in a straight channel with identical flow and sediment characteristics. Two distinct flow regimes were experimentally detected depending on α falling above or below a threshold value α_c in the range of 20–40°. For $\alpha < \alpha_c$ the train of free bars migrates even after reaching an apparently 'naturally stable' state where they are perfectly in phase with steady forced bars. For $\alpha > \alpha_c$ free bars cease migration. The latter state was detected from the disappearance of any bed oscillation in time at any given cross-section. The value of α_c was found to vary with channel meander wavelength L_m^*.

KM's results suggest that it is the interaction between migrating free and steady forced bars which is responsible for the suppression of the former perturbations. Furthermore for suppression to occur, the amplitude of forced bars, which increases with α, must exceed a threshold value dependent on the meander wavelength. A theoretical interpretation of the process, which is also able to provide a predictive tool for engineering purposes, preliminarily requires a finite-amplitude representation of free bars. The latter was obtained in CST as a weakly nonlinear expansion in terms of a small parameter ϵ defined as a measure of the distance from the marginal conditions for free bar formation.

A finite-amplitude representation of forced bars is also required in terms of some dimensionless parameter ν, to be precisely defined, measuring curvature effects.

In the present paper we investigate the interaction of free and forced bars with the

aim of interpreting KM's results and show that, within some range of meander wavenumbers, a critical channel curvature exists for a given set of flow and sediment parameters such that free bars are indeed suppressed. This result also has some practical importance, suggesting how channels might be artificially corrected in order to prevent the occurrence of free bars.

Section 2 is devoted to the formulation of the mathematical model. In §3 its solution is given as a perturbation expansion in terms of the free and forced small parameters (ϵ and ν respectively). An amplitude equation describing the development of free bars in meandering channels is derived in §4 and a discussion of its solution follows in §5. Finally, §6 is devoted to some concluding remarks.

The dual problem mentioned above, namely the influence of free bars initially formed in the originally straight channel on bend instability is outlined in Seminara & Tubino (1989).

2. Formulation of the problem

2.1. *Geometrical preliminaries*

In order to describe flow and bed topography in curved channels it is convenient to adopt a curvilinear coordinate system such that the longitudinal coordinate follows the direction of the main flow. We define the channel axis in parametric form:

$$P(s^*):(X^*_a(s^*), Y^*_a(s^*), Z^*_a(s^*)),$$

with s^* the curvilinear coordinate denoting the arclength (see figure 1).

Let us assume the slope of the channel axis $S \equiv \sin(\theta_s) = -(\mathrm{d}Z^*_a/\mathrm{d}s^*)$ to be constant and denote by (s^*, n^*, z^*) an orthogonal coordinate system such that n^* is horizontal and z^* is directed upward. The metric coefficients of the latter system are readily obtained in the form:

$$h^*_s = (X^{*2}_{,s^*} + Y^{*2}_{,s^*} + Z^{*2}_{,s^*})^{\frac{1}{2}} = 1 + \frac{n^*}{\cos(\theta_s)} r_0^{*-1}(s^*), \tag{1a}$$

$$h^*_n = (X^{*2}_{,n^*} + Y^{*2}_{,n^*} + Z^{*2}_{,n^*})^{\frac{1}{2}} = 1, \tag{1b}$$

$$h^*_z = (X^{*2}_{,z^*} + Y^{*2}_{,z^*} + Z^{*2}_{,z^*})^{\frac{1}{2}} = \cos(\theta_s), \tag{1c}$$

having employed the following relationships for the Cartesian coordinates (X^*, Y^*, Z^*) in terms of (s^*, n^*, z^*)

$$X^* = X^*_a - \frac{n^*}{\cos(\theta_s)} Y^*_{a,s^*}, \quad Y^* = Y^*_a - \frac{n^*}{\cos(\theta_s)} X^*_{a,s^*}, \tag{2a, b}$$

$$Z^* = Z^*_a + z^* \cos(\theta_s), \tag{2c}$$

and having assumed that $(r^*_0)^{-1}$, the curvature of the channel axis, be positive when the centre of curvature lies along the negative n^*-axis.

If the slope of the channel is very small, as is typical of meandering rivers, the metric coefficients have the form (1) with $\cos(\theta_s)$ set equal to 1.

In the following we consider wide channels characterized by variable curvature and focus our attention on the case, vastly explored in the literature, when the channel axis is described by a so-called 'sine generated curve' (figure 2). Thus let us set:

$$\frac{R^*_0}{r^*_0} = r_0^{-1}(s) = e_1 + \text{c.c.} = \exp(\mathrm{i}\lambda_m s) + \text{c.c.}, \tag{3a–c}$$

$$\nu = \frac{B^*}{R^*_0}, \tag{4}$$

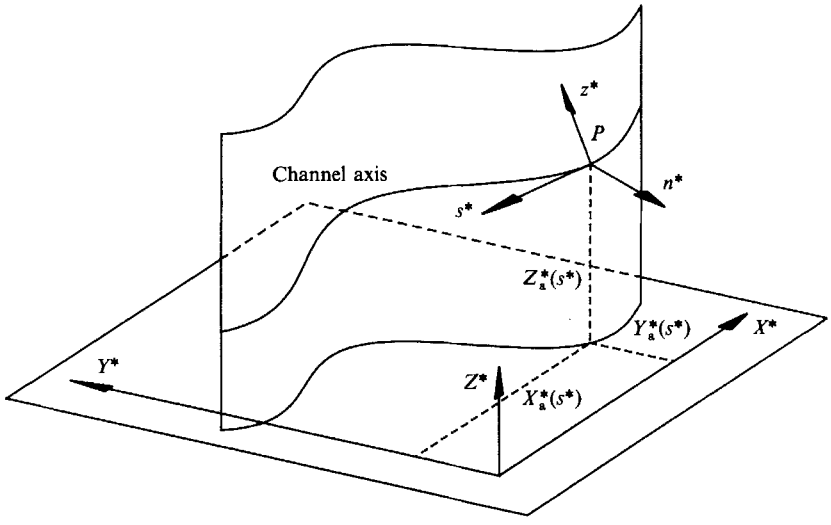

FIGURE 1. Geometrical sketch of the coordinate system.

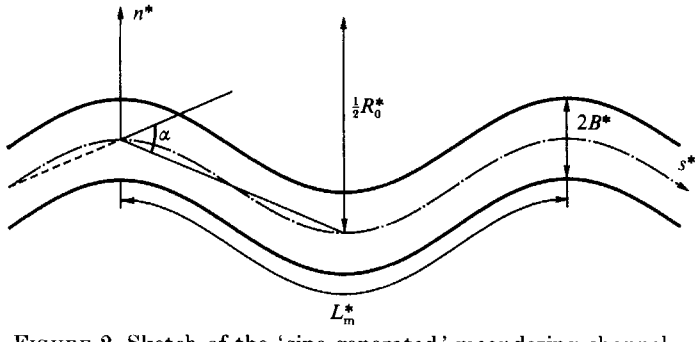

FIGURE 2. Sketch of the 'sine generated' meandering channel.

where B^* is the half-width of the channel, R_0^* is twice the radius of curvature at the bend apex, c.c. (or an overbar in the following) denotes the complex conjugate of a complex number, λ_m and s are the meander wavenumber and longitudinal coordinate both scaled by B^*. Let the bed surface η^* be defined by the following relationship

$$\mathscr{A}^* = z^* - \eta^*(s^*, n^*) = 0. \tag{5}$$

The plane locally tangent to the erodible boundary (figure 3) intersects the reference plane (s^*, z^*) along a straight line. We denote by $\hat{\boldsymbol{\tau}}_1$ the unit vector of the latter while $\hat{\boldsymbol{\nu}}$ denotes the unit vector of the upward direction normal to the tangent plane. Finally let $\hat{\boldsymbol{\tau}}_2$ be the unit vector of the Cartesian axis lying on the tangent plane and orthogonal to $\hat{\boldsymbol{\tau}}_1$ and $\hat{\boldsymbol{\nu}}$. It is readily shown that $(\hat{\boldsymbol{\nu}}, \hat{\boldsymbol{\tau}}_1, \hat{\boldsymbol{\tau}}_2)$ read:

$$\hat{\boldsymbol{\nu}} = \frac{\left(-\frac{1}{h_s^*}\eta^*_{,s^*}; -\eta^*_{,n^*}; 1\right)}{\left(1+(\eta^*_{,n^*})^2+\left(\frac{1}{h_s^*}\eta^*_{,s^*}\right)^2\right)^{\frac{1}{2}}}, \quad \hat{\boldsymbol{\tau}}_1 = \frac{\left(1; 0; \frac{1}{h_s^*}\eta^*_{,s^*}\right)}{\left(1+\left(\frac{1}{h_s^*}\eta^*_{,s^*}\right)^2\right)^{\frac{1}{2}}}, \tag{6a, b}$$

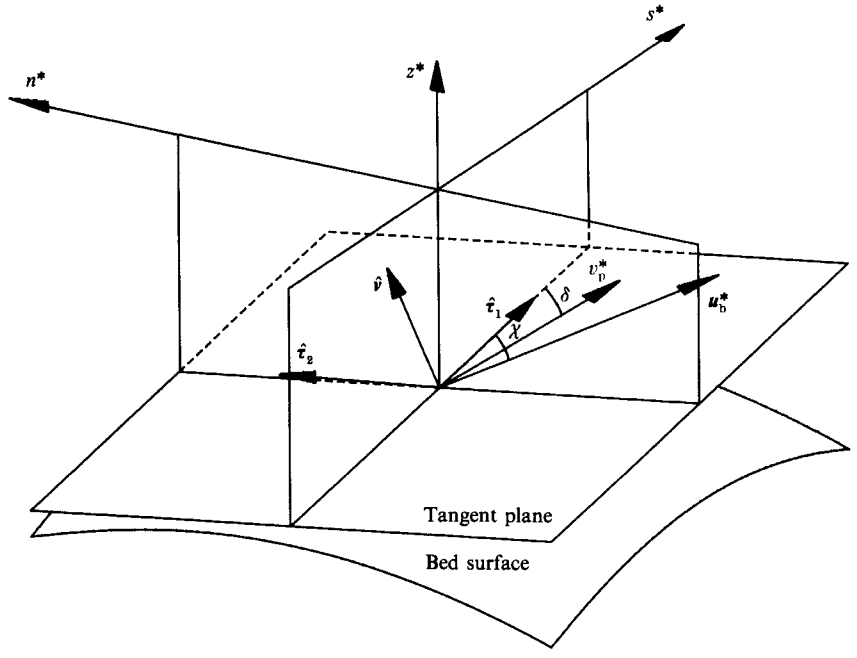

FIGURE 3. Sketch of reference frame (v_p^* = particle velocity, u_b^* = average bottom stress).

$$\hat{\tau}_2 = \frac{\left(-\frac{1}{h_s^*}\eta_{,s^*}^*\eta_{,n^*}^*; 1+\left(\frac{1}{h_s^*}\eta_{,s^*}^*\right)^2; \eta_{,n^*}^*\right)}{\left(\left[1+\left(\frac{1}{h_s^*}\eta_{,s^*}^*\right)^2\right]^2+\left(\frac{1}{h_s^*}\eta_{,s^*}^*\eta_{,n^*}^*\right)^2+(\eta_{,n^*}^*)^2\right)^{\frac{1}{2}}}. \tag{6c}$$

The above relationships will be employed in order to derive the Cartesian components of bed load after the direction of bed load transport along the tangent plane has been established.

2.2. *Governing equations*

We assume the channel width ($2B^*$) to be large enough for sidewall effects to be negligible in the central region of the flow. In other words we study the central region of the flow independently of the boundary layers adjacent to the sidewalls. By this scheme, which goes back to Engelund (1974), essentially the existence of two distinct lengthscales for transverse variation of flow quantities is assumed: the channel width which is relevant to the core region and the flow depth which is relevant to the wall region. Furthermore, the latter flow regions are assumed to interact weakly. The validity of this approach is discussed below.

Furthermore, let us recall that free bars contribute little to flow resistance at least for active gravel beds (Shen 1962; Bray 1979; Parker & Peterson 1980; Jaeggi 1984): this implies that flow separation is not likely to be a crucial feature of free bar development. This premise and the work of CST then encourage one to assume an approximate representation of the flow field by means of a depth-averaged model, obviously unable to predict separation but still suitable to model the gross features of flow structure and bed topography. Such a model, though quite complicated, would still provide a manageable tool for investigating analytically complex phenomena involving nonlinear interactions of the type that will be discussed in the following.

However, a proper formulation of a two-dimensional model of flow and bed topography in curved channels requires to account appropriately for the 'dispersive' effects which arise as a consequence of performing the process of depth averaging. This was first pointed out by Kalkwijk & de Vriend (1980). Following ideas originally developed by Engelund (1974) it is convenient to decompose the transverse component of velocity into a helical component with vanishing depth average and a depth-averaged component. Denoting the vertical distributions of these components by $\Gamma_0(z)$ and $\Gamma_1(z)$, respectively, and the vertical distribution associated with the longitudinal component by $F_1(z)$, the velocity field is expressed in the form

$$u = F_1(z;\lambda_m)\,U(s,n), \quad v = \nu[\Gamma_0(z;\lambda_m)\,e_1 + \text{c.c.}]\,U(s,n) + \Gamma_1(z;\lambda_m)\,V(s,n), \quad (7a,b)$$

where quantities are dimensionless as described below (see equation (13)), ν is the curvature ratio defined in (4), (u,v) and (U,V) are local and depth-averaged longitudinal and transverse components of velocity respectively. In order to include dispersive effects into the differential problem for the depth-averaged flow field we must assume a vertical structure for F_1, Γ_0 and Γ_1. In the following we will employ expressions for F_1, Γ_0, Γ_1 as they emerge from the results of a fully three-dimensional linear model (Seminara & Tubino 1985, 1989). In particular F_1 and Γ_1 are found to coincide with the uniform unperturbed velocity distribution $u_0(z)$.

Thus equations (7*a* and *b*) take the form:

$$u = u_0(z)\,U(s,n), \quad v = \nu[\Gamma_0(z;\lambda_m)\,e_1 + \text{c.c.}]\,U(s,n) + u_0(z)\,V(s,n). \quad (8a,b)$$

The validity of the above decomposition is only approximate: indeed the vertical distributions associated with the depth-averaged components of u and v coincide with $u_0(z)$ only at a linear level and in the limit $\lambda_m \to 0$ when the effect of longitudinal convection vanishes. It may be expected that the analysis will not be largely affected by the latter assumption since longitudinal convection is still accounted for in the depth-averaged model and is only neglected in the evaluation of the latter dispersive effects. The approximations associated with the decomposition (8*a*, *b*) are the price to pay for reducing the complexity of the problem from that of a three-dimensional approach to that of a more tractable two-dimensional scheme.

Also notice that the decomposition (8*a*, *b*) differs slightly from that originally proposed by Kalkwijk & de Vriend (1980) in that the longitudinal convection term is kept in the equation for $\Gamma_0(z)$ (Seminara & Tubino 1985, 1989) as it is appropriate to the present context where the local curvature of the channel axis varies in the longitudinal direction. Mathematically this implies that the function $\Gamma_0(z)$ is complex. Physically, the imaginary part of $\Gamma_0(z)$ describes the lag required for secondary flow to adapt to local curvature. This effect was accounted for by de Vriend (1981) by introducing a damping exponential function characterized by some 'relaxation length' to describe the adaptation process of secondary flow. Though the latter procedure was not incorporated within the framework of a rational perturbation procedure it does not differ substantially from the present approach.

Finally we point out that, denoting by β the width ratio of the channel (see (14*b*)), the approach employed herein whereby the sidewall boundary layers are ignored, is justified as the leading-order approximation of an expansion in powers of the small parameter β^{-1}, but requires some care. In fact, it has been shown by de Vriend (1981) that ignoring the sidewall boundary layers may affect the transverse redistribution of longitudinal momentum in a non-negligible way if the channel has steep sidewalls and is not shallow enough. More recently Johannesson & Parker (1989) have shown

by an appropriate procedure that the neglected term in the longitudinal momentum equation may be estimated to be $O(\sigma/\beta^2)$ smaller than the remaining ones. However, the coefficient σ may attain values of a few hundreds. Thus, though neglecting the latter contribution is formally justified at leading order in the expansion in terms of (β^{-1}), the approximation may be poor if β is not large enough, i.e. if the channel is not shallow enough. It should also be noticed that the above effect is less significant for rivers characterized by banks which are not very steep.

By substituting from $(8a, b)$ into the three-dimensional Reynolds equations written in the present coordinate system, performing depth integration and keeping only longitudinal and transverse shear stresses we find the following differential equations for the depth-averaged component of the flow field

$$UU_{,s}+VU_{,n}+H_{,s}+\frac{\beta\tau_s}{D}=-\nu\mathscr{R}(s)\left[n\left(\frac{\beta\tau_s}{D}+VU_{,n}\right)+UV\right]$$
$$-\nu\mathscr{R}_1(s)\frac{1}{D}(U^2D)_{,n}-\nu^2\mathscr{R}_2(s)\left[\frac{n}{D}(U^2D)_{,n}+2U^2\right], \quad (9)$$

$$UV_{,s}+VV_{,n}+H_{,n}+\beta\frac{\tau_n}{D}=-\nu\mathscr{R}(s)\left[n\left(VV_{,n}+H_{,n}+\frac{\beta\tau_n}{D}\right)-U^2\right]$$
$$-\nu\mathscr{R}_1(s)\left\{\frac{1}{D}[(DU^2)_{,s}+2(UDV)_{,n}]\right\}-\nu(\mathrm{i}\lambda_m k_1 e_1+\mathrm{c.c.})\,U^2$$
$$-2\nu^2\mathscr{R}_2(s)\left[\frac{n}{D}(UVD)_{,n}+UV\right]-\nu^2\mathscr{R}_3(s)\frac{1}{D}(U^2D)_{,n}, \quad (10)$$

$$(DU)_{,s}+(DV)_{,n}=-\nu\mathscr{R}(s)\,[VD+n(DV)_{,n}], \quad (11)$$

$$(F_0^2H-D)_{,t}+Q_0(Q_{s,s}+Q_{n,n})=-Q_0\frac{\nu\mathscr{R}(s)}{1+\nu n\mathscr{R}(s)}(Q_n-nQ_{s,s}), \quad (12)$$

where t is time, H is free-surface elevation, D is local depth, (τ_s, τ_n) and (Q_s, Q_n) are bottom shear stresses and sediment flow rate components in the longitudinal and transverse directions.

The variables have been made dimensionless in the form:

$$(u^*, v^*, U^*, V^*)=U_0^*(u, v, U, V), \quad (H^*, D^*, \eta^*, z^*)=D_0^*(F_0^2H, D, \eta, z), \quad (13a, b)$$

$$(s^*, n^*)=B^*(s, n), \quad (\tau_s^*, \tau_n^*)=\rho U_0^{*2}(\tau_s, \tau_n), \quad (13c, d)$$

$$(Q_s^*, Q_n^*)=d_s^*\left\{\left(\frac{\rho_s}{\rho}-1\right)gd_s^*\right\}^{\frac{1}{2}}(Q_s, Q_n), \quad t^*=\frac{B^*}{U_0^*}t, \quad (13e, f)$$

where ρ_s and d_s^* are density and diameter of the sediment modelled as uniform, ρ is water density, g is gravitational acceleration, U_0^*, D_0^* and F_0 are averaged speed, depth and Froude number for the uniform unperturbed flow.

Furthermore Q_0 is the ratio between the scale of sediment discharge and the flow rate and β is width ratio defined as

$$Q_0=d_s^*\frac{\{(\rho_s/\rho-1)\,gd_s^*\}^{\frac{1}{2}}}{(1-p)\,D_0^*\,U_0^*}, \quad \beta=\frac{B^*}{D_0^*}, \quad (14a, b)$$

where p denotes sediment porosity.

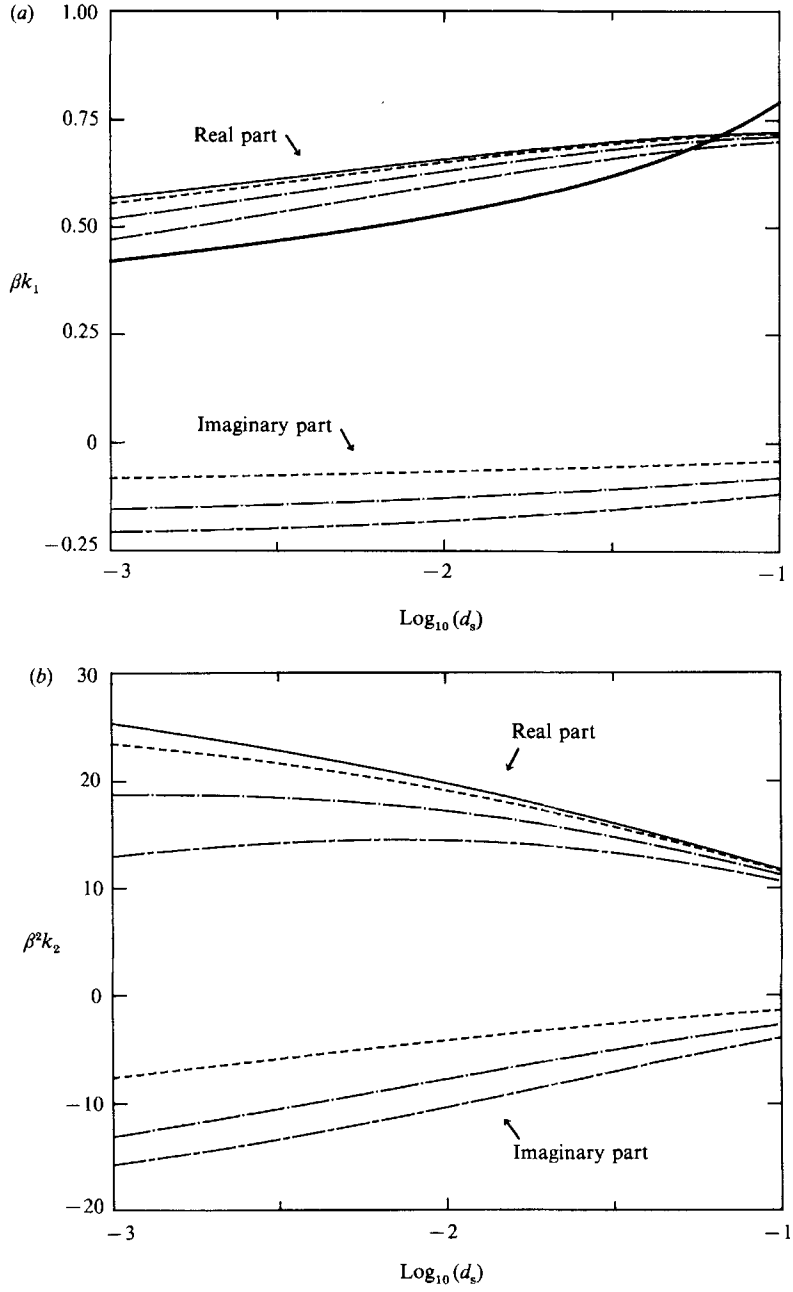

FIGURE 4(*a*, *b*). For caption see facing page.

Finally

$$\mathscr{R}(s) = e_1 + \text{c.c.}, \quad \mathscr{R}_1(s) = k_1 e_1 + \text{c.c.}, \quad \mathscr{R}_2(s) = k_1 e_2 + k_1 + \text{c.c.}, \qquad (15a\text{–}c)$$

$$\mathscr{R}_3(s) = k_2 e_2 + k_3 + \text{c.c.}, \quad e_j = \exp[j(\mathrm{i}\lambda_m s)] \quad (j = 1, 2, \ldots). \qquad (15d, e)$$

The parameters k_1, k_2 and k_3, arising from the velocity decomposition (8*a*, *b*), have the following form:

$$k_1 = \frac{1}{D}\int_\eta^{F_0^2 H} u_0 \Gamma_0 \, \mathrm{d}z, \quad k_2 = \frac{1}{D}\int_\eta^{F_0^2 H} \Gamma_0^2 \, \mathrm{d}z, \quad k_3 = \frac{1}{D}\int_\eta^{F_0^2 H} |\Gamma_0|^2 \, \mathrm{d}z. \qquad (16a\text{–}c)$$

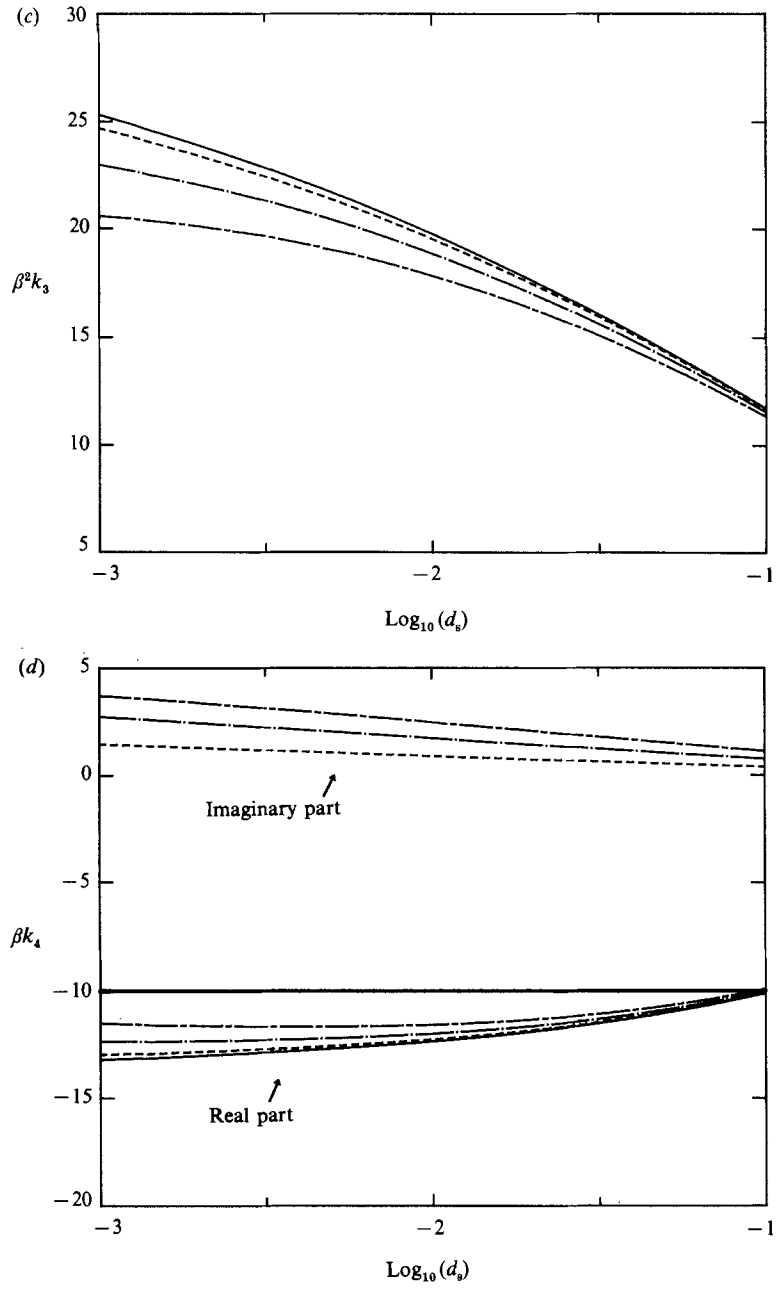

FIGURE 4. The parameters βk_1, $\beta^2 k_2$, $\beta^2 k_3$, βk_4, are plotted versus the grain ratio d_s for given values of the meander wavenumber $\lambda_m(\beta = 30)$. ——, $\lambda_m = 0$; – – – – –, $\lambda_m = 0.2$; —·—, $\lambda_m = 0.4$; ———, $\lambda_m = 0.6$; (*a*) ——, Kalkwijk & de Vriend (1980); (*d*) ——, Engelund (1974).

They are plotted versus the non-dimensional sediment diameter $d_s = (d_s^*/D_0^*)$ for given values of the meander wavenumber λ_m in figure (4) where previous results by Kalkwijk & de Vriend (1980) and Engelund (1974) are also reported.

Notice that the timescale B^*/U_0^* is appropriate for the flow field. From (12) it appears that the morphological timescale is $(Q_0)^{-1}$ larger than the flow timescale. Since typical values of Q_0 are in the range 10^{-3}–10^{-5} it follows that a quasi-steady

approach, whereby the flow field is assumed to adapt instantaneously to changes in the bottom configuration, is appropriate to the present context.

2.3. *Boundary and integral conditions*

We ignore the sidewall boundary layers and require the channel walls to be impermeable both to the flow and to the sediment. Thus we set

$$V = Q_n = 0 \quad (n = \pm 1). \tag{17a, b}$$

Furthermore, we introduce appropriate integral conditions which express the requirements that flow discharge per unit width and averaged reach slope should not be altered by the development of perturbations. We write:

$$\int_{-1}^{1} UD \, \mathrm{d}n = 2, \quad \int_{0}^{2\pi/\lambda_m} \mathrm{d}s \int_{-1}^{1} (F_0^2 H - D) \, \mathrm{d}n = \text{const.} \tag{18a, b}$$

2.4. *Bottom stresses*

Having ignored separation we model the flow structure as slowly varying both in space and in time. This suggests that the bottom stress, modelled as aligned with the near bed velocity vector, be expressed in terms of a local friction coefficient C defined by the relationships

$$\boldsymbol{\tau} = (\tau_s, \tau_n) = (U, V + \nu U(k_4 e_1 + \text{c.c.}))\,(U^2 + V^2)^{\frac{1}{2}} C, \tag{19a}$$

$$k_4 = \left[\frac{\Gamma_{0,z}}{u_{0,z}}\right]_\eta. \tag{19b}$$

In the following the local bed configuration will be assumed to be plane so that the following logarithmic formula will be employed for the friction coefficient:

$$C^{-\frac{1}{2}} = 6 + 2.5 \ln\left(\frac{D}{2.5 d_s}\right), \quad d_s = \frac{d_s^*}{D_0^*}, \tag{20a, b}$$

where the roughness parameter has been put equal to $(2.5 \mathrm{d}_s^*)$ after Engelund & Hansen (1967).

We point out explicitly that this procedure is equivalent to assuming that the turbulent structure is in equilibrium with the local conditions, its spatial and velocity scales being the local values of depth and friction velocity respectively. This model is likely to be approximately adequate anywhere but in the weak separation zone.

2.5. *Sediment transport*

For the sake of simplicity we assume sediment to be transported mainly as bed load. An extension to the case where a significant fraction of sediment is transported in suspension seems feasible though it may require a more refined (possibly fully three-dimensional) description of the flow field in the near bank regions where vertical velocities are significant.

Sediment transport is assumed to be determined by local flow conditions, its direction deviating from the direction of average bottom stress under the action of gravity. In non-dimensional form we write (see figure 3)

$$\boldsymbol{Q} = (Q_{\tau 1}, Q_{\tau 2}, Q_\nu) = (\cos\delta, \sin\delta, 0)\, \Phi, \tag{21}$$

where Φ is the dimensionless equilibrium bed load function evaluated locally.

For relatively small values of δ the experiments of Ikeda (1982) (see also Parker's (1984) discussion) suggest the following formula

$$\sin\delta = \sin\chi - \frac{r}{\beta\theta^{\frac{1}{2}}}(F_0^2 H - D)_{,n}, \tag{22}$$

to be appropriate, where χ is the angle between bottom stress and the $\hat{\boldsymbol{\tau}}_1$-direction, θ is the local Shields parameter and r is a coefficient (presumably dependent on the particle Reynolds number) which various authors suggest taking as a constant ranging between 0.3 (Olesen 1983) and 0.54 (Engelund 1981).

Equation (22) has been satisfactorily employed in most theoretical works on morphological evolution of cohesionless channels. Thus, it does not lack substantiation. It is, however, appropriate to point out its empirical character, though successful attempts to derive an expression of the same type as (22) have been proposed in the literature (Kikkawa, Ikeda & Kitagawa 1976; Engelund 1981; Parker & Andrews 1985), all of them are based on somewhat 'averaged' models of sediment grain dynamics along curved paths. Furthermore, (22) can only be appropriate within a linear context. An extension of (22) to the weakly nonlinear case would possibly be more appropriate to the present context. However, effects of nonlinearity of (22) have been found by the authors to be fairly weak such that it does not seem to be convenient to further complicate the analysis given the uncertainty which is still present in the estimate of the coefficient r. The latter has often been based on measurements of transverse bed slope in fully developed flow in constant curvature rectangular channels with erodible bed and on estimates of $\sin(\chi)$ based on theoretical models which are linear and apply to fairly wide channels. The latter conditions are only approximately satisfied in the experiments.

The Meyer Peter Müller formula in the form given by Chien (1954) will be employed to evaluate Φ. Thus:

$$\Phi = 8(\theta - \theta_{\rm cr})^{\frac{3}{2}}, \quad \theta_{\rm cr} = 0.047. \tag{23a, b}$$

Finally the longitudinal and transverse components of $\boldsymbol{Q}$ are derived from $Q_{\tau 1}$ and $Q_{\tau 2}$ using (6*b*, *c*). We find:

$$Q_s = Q_{\tau 1}\left[1 - \frac{1}{2}\left(\frac{\eta_{,s}}{\beta(1+\nu n\mathscr{R}(s))}\right)^2\right] - Q_{\tau 2}\frac{\eta_{,s}\eta_{,n}}{\beta^2(1+\nu n\mathscr{R}(s))}, \tag{24}$$

$$Q_n = Q_{\tau 2}\left[1 - \frac{1}{2}\left(\frac{\eta_{,n}}{\beta}\right)^2\right], \tag{25}$$

having neglected fourth-order terms in the products between the longitudinal and transverse slopes.

3. Expansion

We now wish to determine the solution for flow and bed topography in a weakly meandering channel where free and forced bars are assumed to coexist. It will appear that our solution will allow us to ascertain the conditions for the above coexistence to be possible.

The 'weak meandering' assumption is mathematically expressed in the form

$$\nu \ll 1. \tag{26}$$

In this respect it should be noticed that the critical values of the curvature ratio ν

for free bar suppression observed by KM never exceeded 0.1, which suggests the suitability of the present approach to interpret KMs experimental observations. Now the structure of flow and bed topography in weakly meandering shallow channels in the absence of free bars has been the subject of many investigations (see Seminara & Tubino (1989) for a review). Most of them take advantage of the weak effects of curvature by expanding the solution for (U, V, H, D) far from the banks in powers of ν in the following typical form given for U:

$$U = 1 + \underbrace{\nu[e_1 U_1(n) + \text{c.c.}] + \nu^2\{[e_2 U_2(n) + \text{c.c.}] + U_0(n)\}}_{\text{forced response}} + O(\nu^3). \tag{27}$$

The part of solution (27) representing the perturbation with respect to the uniform flow will be referred to in the following as the 'forced response' of the channel. Its linear part is essentially the steady 'forced bar' solution derived in BS. The $O(\nu^2)$ terms arise from nonlinear interactions and consist of a second harmonic in the longitudinal direction (term proportional to U_2) and a distortion of the basic uniform flow (term proportional to U_0).

On the other hand if channel curvature is ignored and the channel is assumed to be wide enough for its width ratio β to exceed the critical value β_c below which free bars are damped, an instability process occurs which leads to the development of large-scale migrating perturbations called alternate (or free) bars. Linear stability of free bars has been investigated in the seventies in an increasingly refined fashion starting from the work of Callander (1969). Such a theory allows one to predict:

(i) the dependence of the critical width ratio β_c on unperturbed Shields stress θ_0 and the grain roughness d_s;

(ii) the wavenumber λ_c of the bar characterized by maximum growth rate, i.e. the most suitable candidate to occur in practice;

(iii) the angular frequency ω_c of the fastest growing perturbation.

Thus the structure of free bar perturbations predicted by linear theory is given in the form

$$(U, V, H, D) \propto \exp(\Omega t)\,(u_1 S_1, v_1 C_1, h_1 S_1, d_1 S_1) E_1 + \text{c.c.}, \tag{28}$$

where (u_1, v_1, h_1, d_1) are infinitesimal amplitudes, Ω is the bar growth rate (vanishing at critical conditions) and the following notations are employed

$$S_m(n) = \sin(\tfrac{1}{2}mn\pi), \quad C_m(n) = \cos(\tfrac{1}{2}mn\pi) \quad (m = 1, 2, \ldots) \tag{29a, b}$$

$$E_j = \exp[ji(\lambda s - \omega t)] \quad (j = 1, 2, \ldots), \tag{29c}$$

where the dimensionless bar wavenumber λ and angular frequency ω are scaled by $(1/B^*)$ and (U_0^*/B^*) respectively.

The linear dispersion relationship obtained from linear theory is of the type:

$$\Omega = \Omega(\lambda, \omega, \beta; \theta_0, d_s). \tag{30}$$

This allows the predictions (i), (ii) and (iii).

The indefinite growth predicted by linear theory for $\beta > \beta_c$ (supercritical conditions) is inhibited by nonlinear effects which give rise to a supercritical bifurcation. This was shown by the weakly nonlinear theory of CST. In the latter work the nonlinear development of the linear solution (28) was followed for values of β close enough to the critical value β_c. Having defined the small parameter ϵ in the form

$$0 < \epsilon \equiv \frac{\beta - \beta_c}{\beta_c} \ll 1, \tag{31}$$

it was shown that in such a weakly nonlinear regime:

(i) the linear growth rate Ω is $O(\epsilon)$, i.e. it can be written as $(\Omega_1 \epsilon)$ with $\Omega_1 \sim O(1)$;
(ii) the growth of perturbations is described by the slow time variable

$$T = \epsilon t, \tag{32}$$

such that a characteristic amplitude or bar perturbation is $A(T)$;

(iii) as $T \to -\infty$, $A(T)$ tends to $\exp(\Omega_1 T)$ in accordance with linear theory, whereas as $T \to \infty$ it is found that A tends to an equilibrium value A_e asymptotically reached.

The structure of free bars in this weakly nonlinear regime can be inferred from the following expansion for U:

$$\left.\begin{aligned} U = {} & 1 \qquad\qquad\qquad\qquad\qquad\qquad \} \text{uniform flow} \\ & + \epsilon^{\frac{1}{2}}[A(T) S_1 E_1 u_1 + \text{c.c.}] \\ & + \epsilon\{[A^2 E_2 (u_{22} C_2 + u_{02}) + \text{c.c.}] + A\bar{A}(u_{20} C_2 + u_{00})\} \} \text{free response} \\ & + \epsilon^{\frac{3}{2}}[S_1 E_1 u_{11}(T) + \text{c.c.}] + O(\epsilon^{\frac{3}{2}}), \end{aligned}\right\} \tag{33}$$

where E_1 and E_2 are given by (29*c*) with λ and ω replaced by λ_c and ω_c.

The order of magnitude of the fundamental perturbations is found to be $\epsilon^{\frac{1}{2}}$ from a classical argument of hydrodynamic stability whereby secular terms originated by nonlinear interactions at third order must be prevented (see CST, p. 220). It appears from (33) that nonlinearity gives rise at second order (ϵ) to a (migrating) second harmonic proportional to E_2 and a distortion of the basic uniform flow. At third order ($\epsilon^{\frac{3}{2}}$) the fundamental is reproduced.

The part of (33) representing the perturbation of the basic uniform flow will be referred to in the following as the 'free response' of the channel.

The above premise now allows us to seek a weakly nonlinear solution in the regime defined by (26) and (31) where free and forced bars are assumed to coexist. A natural extension of (27) and (33) in this case is of the form:

$$\left.\begin{aligned} U = {} & \text{uniform flow} + \text{free response} + \text{forced response} \\ & + \nu\epsilon^{\frac{1}{2}}\{[A E_1 e_1 U_{11}(n) + \overline{A E}_1 e_1 \hat{U}_{11}(n)] + \text{c.c.}\} \\ & + \nu^2 \epsilon^{\frac{1}{2}}[A E_1 U_{10}(n) + \text{c.c.}] \\ & + O(\nu^2 \epsilon^{\frac{1}{2}}, \nu\epsilon). \end{aligned}\right\} \text{mixed response} \tag{34}$$

Similar expansions are assumed for $(V, H, D, \tau_s, \tau_n, Q_s, Q_n)$ (and obviously for Φ, θ and C). A few comments are needed to clarify the structure of (34).

The mixed component of (34) arises at second order $O(\nu\epsilon^{\frac{1}{2}})$ from the direct interaction between the fundamental free mode (migrating) and the fundamental forced mode (steady) giving rise to a migrating component. Further mixed interactions lead to reproducing the fundamental free mode at $O(\nu^2\epsilon^{\frac{1}{2}})$. From the work of CST we know that the latter is also reproduced at $O(\epsilon^{\frac{3}{2}})$ by free interactions (see expansion (33)) and indeed this leads to the appearance of secular terms, the suppression of which determines the structure of the amplitude equation governing the development of the function $A(T)$. It follows that, provided $\epsilon^{\frac{3}{2}} \sim \nu^2\epsilon^{\frac{1}{2}}$ or $\epsilon^{\frac{1}{2}} \sim \nu$, the effect of mixed interactions is felt directly by the amplitude equation. Physically this implies that the growth of free bars is influenced strongly by curvature provided the amplitude of free bars ($O(\epsilon^{\frac{1}{2}})$) and forced bars ($O(\nu)$) be comparable.

Whether the latter effect is going to reinforce or damp the development of free bars can only be ascertained by substituting from the expansion (34) into the governing

differential problem, solving the differential system obtained at various orders and deriving the modified structure of the amplitude equation arising at $O(\epsilon^{\frac{3}{2}}, \nu^2\epsilon^{\frac{1}{2}})$.

Before outlining this procedure, we point out that the condition $\epsilon^{\frac{1}{2}} \sim \nu$ for free bar growth to be affected by curvature could also be derived within the context of a linear stability theory of free bar formation in a curved erodible channel. In fact, two things affect the growth rate of free bars in curved channels close to the critical conditions of the straight channel case. The former is the distance from the latter conditions: if ϵ is a measure of this distance, the contribution to the growth rate of free bars associated with the former effect is $O(\epsilon)$ and destabilizing if $\beta > \beta_c$. A second contribution arises from the modifications of the basic flow with respect to uniform straight channel flow. Such modifications can be represented by expanding the basic flow in powers of the curvature ratio ν. Correspondingly linear free bar perturbations of the basic flow would have to be expanded in powers of ν. A simple argument would then show that an $O(\nu^2)$ correction for the growth rate of the fundamental is required to prevent the occurrence of secular terms in the $O(\nu^2)$ system for the perturbations. The latter contribution to the growth rate may be destabilizing or stabilizing but balance with the former contribution is only possible provided $\nu^2 \sim \epsilon$, i.e. $\nu \sim \epsilon^{\frac{1}{2}}$ as previously found.

4. Outline of the perturbation procedure

We now give the differential systems governing the solution at various orders. Their derivation involves a large amount of tedious algebra. Details of the calculations, in particular the expressions for third-order components of $(\tau_s, \tau_n, Q_s, Q_n)$ in terms of components of (U, V, H, D) are reported in Appendix B available from the *Journal of Fluid Mechanics* Editorial Office.

4.1. *Free mode*

The differential systems governing the free mode components at $O(\epsilon^{\frac{1}{2}})$ and $O(\epsilon)$ and their solutions are identical with the corresponding ones obtained in CST. We then refer the reader to the latter paper.

4.2 *Forced mode*

$O(\nu)$

The differential problem governing the fundamental forced mode at $O(\nu)$ is very close to that obtained by BS; slight differences arising from some small dispersive effects associated with the zero depth average component of transverse velocity which was neglected in BS. We then find

$$\mathrm{L}_1 \begin{pmatrix} U_1 \\ V_1 \\ H_1 \\ D_1 \end{pmatrix} = \begin{pmatrix} b_1^{(1)} \\ b_2^{(1)} \\ b_3^{(1)} \\ b_4^{(1)} \end{pmatrix}, \tag{35a–d}$$

$$V_1 = R(F_0^2 H_1 - D_1)_{,n} - k_4 = 0 \quad (n = \pm 1), \tag{35e,f}$$

where

$$\mathrm{L}_1 \equiv \begin{pmatrix} a_{11} & a_{12} & a_{13} & a_{14} \\ a_{21} & a_{22} & a_{23} & a_{24} \\ a_{31} & a_{32} & a_{33} & a_{34} \\ a_{41} & a_{42} & a_{43} & a_{44} \end{pmatrix}, \tag{35g}$$

and the coefficients $a_{ij}(i,j=1,4)$ and $b_j^{(1)}(j=1,4)$ read:

$$a_{11}=\mathrm{i}\lambda_m+\beta_c C_0 s_1,\quad a_{12}=a_{21}=a_{24}=a_{33}=0, \tag{36a–e}$$

$$a_{13}=a_{31}=a_{34}=\mathrm{i}\lambda_m,\quad a_{14}=\beta_c C_0(s_2-1), \tag{36f–i}$$

$$a_{22}=\mathrm{i}\lambda_m+\beta_c C_0,\quad a_{23}=a_{32}=a_{42}=\frac{\mathrm{d}}{\mathrm{d}n}, \tag{36j–m}$$

$$a_{41}=\mathrm{i}\lambda_m f_1,\quad a_{43}=-F_0^2 R\frac{\mathrm{d}^2}{\mathrm{d}n^2},\quad a_{44}=\mathrm{i}\lambda_m f_2+R\frac{\mathrm{d}^2}{\mathrm{d}n^2}, \tag{36n–p}$$

$$b_1^{(1)}=-n\beta_c C_0,\quad b_2^{(1)}=1-\mathrm{i}\lambda_m k_1-\beta_c C_0 k_4,\quad b_3^{(1)}=b_4^{(1)}=0. \tag{36q–t}$$

In (36*a–t*) the following notations have been employed:

$$s_1=2(1-C_T)^{-1},\quad s_2=C_D(1-C_T)^{-1}, \tag{37a, b}$$

$$f_1=\frac{2\Phi_T}{1-C_T},\quad f_2=\Phi_D+\frac{C_D\Phi_T}{1-C_T},\quad R=\frac{r}{\beta(\theta_0)^{\frac{1}{2}}}, \tag{37c–e}$$

with

$$C_D=\frac{1}{C_0}\frac{\partial C}{\partial D},\quad C_T=\frac{\theta_0}{C_0}\frac{\partial C}{\partial\theta},\quad \Phi_D=\frac{1}{\Phi_0}\frac{\partial\Phi}{\partial D},\quad \Phi_T=\frac{\theta_0}{\Phi_0}\frac{\partial\Phi}{\partial\theta}, \tag{38a–d}$$

θ_0, C_0 and Φ_0 being Shields parameter, friction coefficient and bed load function of unperturbed uniform flow.

The solution of (35*a–f*) can readily be obtained in closed form as described in BS. (Notice that in the latter paper an algebraic error was contained in equation (39*d*) which was corrected in Blondeaux & Seminara 1988).

$O(\nu^2)$

The differential system governing the second harmonic of the forced mode reads

$$\mathrm{L}_2\begin{pmatrix}U_2\\V_2\\H_2\\D_2\end{pmatrix}=\begin{pmatrix}b_1^{(2)}\\b_2^{(2)}\\b_3^{(2)}\\b_4^{(2)}\end{pmatrix}, \tag{39a–d}$$

$$V_2=R(F_0^2H_2-D_2)_{,n}-Q'_{n2}=0\quad(n=\pm1), \tag{39e, f}$$

while the distortion of the basic flow is obtained as the solution of the following system

$$\mathrm{L}_0\begin{pmatrix}U_0\\V_0\\H_0\\D_0\end{pmatrix}=\begin{pmatrix}b_1^{(0)}\\b_2^{(0)}\\b_3^{(0)}\\b_4^{(0)}\end{pmatrix}, \tag{40a–d}$$

$$V_0=R(F_0^2H_0-D_0)_{,n}-Q'_{n0}=0\quad(n=\pm1), \tag{40e, f}$$

$$\int_{-1}^{1}[U_0+D_0+(U_1\bar{D}_1+\text{c.c.})]\,\mathrm{d}n=0,\quad \int_{-1}^{1}(F_0^2H_0-D_0)\,\mathrm{d}n=0, \tag{40g, h}$$

where $L_j (j = 0, j = 2)$ is a linear differential operator obtained from L_1 by replacing λ_m with $(j\lambda_m)$ and the coefficients $b_j^{(2)}(n)$ and $b_j^{(0)}(n)$ $(j = 1, 4)$ read:

$$b_1^{(2)} = -i\lambda_m U_1^2 - V_1(1+U_{1,n}) - k_1(2U_{1,n}+D_{1,n}+2) - \beta_c C_0[T'_{s2}+n(T_{s1}-D_1)+D_1(D_1-T_{s1})], \quad (41a)$$

$$b_2^{(2)} = -i\lambda_m U_1 V_1 - V_1 V_{1,n} + 2U_1 - k_1[2V_{1,n}+i\lambda_m(4U_1+D_1)] - nH_{1,n} - \beta_c C_0[T'_{n2}+T_{n1}(n-D_1)], \quad (41b)$$

$$b_3^{(2)} = -2i\lambda_m D_1 U_1 - V_{1,n}(n+D_1) - V_1(1+D_{1,n}), \quad (41c)$$

$$b_4^{(2)} = -2i\lambda_m Q'_{s2} - Q'_{n2} + ni\lambda_m Q_{s1} - Q_{n1}, \quad (41d)$$

$$b_1^{(0)} = \{[-\bar{V}_1(1+U_{1,n}) - \bar{k}_1(2U_{1,n}+D_{1,n}+2) - \beta_c C_0(n(T_{s1}-D_1)+\bar{D}_1(D_1-T_{s1}))] + \text{c.c.}\} - \beta_c C_0 T'_{s0} \quad (41e)$$

$$b_2^{(0)} = \{[-i\lambda_m \bar{U}_1 V_1 - \bar{V}_1 V_{1,n} + 2U_1 - \bar{k}_1(2V_{1,n}+i\lambda_m D_1) - nH_{1,n} - \beta_c C_0 \bar{T}_{n1}(n-D_1)] + \text{c.c.}\} - \beta_c C_0 T'_{n0}, \quad (41f)$$

$$b_3^{(0)} = [-\bar{V}_{1,n}(n+D_1) - \bar{V}_1(1+D_{1,n})] + \text{c.c.}, \quad (41g)$$

$$b_4^{(0)} = [(ni\lambda_m Q_{s1} - Q_{n1}) + \text{c.c.}] - Q'_{n0}. \quad (41h)$$

Notice that the following decompositions have been employed for the $O(\nu^2)$ components of τ_s/C_0, τ_n/C_0, Q_s/Φ_0 and Q_n/Φ_0:

$$T_{s0} = s_1 U_0 + s_2 D_0 + T'_{s0}, \quad T_{s2} = s_1 U_2 + s_2 D_2 + T'_{s2}, \quad (42a, b)$$

$$T_{n0} = V_0 + T'_{n0}, \quad T_{n2} = V_2 + T'_{n2}, \quad (42c, d)$$

$$Q_{s0} = f_1 U_0 + f_2 D_0 + Q'_{s0} \quad Q_{s2} = f_1 U_2 + f_2 D_2 + Q'_{s2}, \quad (42e, f)$$

$$Q_{n0} = V_0 - R\frac{d(F_0^2 H_0 - D_0)}{dn} + Q'_{n0} \quad (42g)$$

$$Q_{n2} = V_2 - R\frac{d(F_0^2 H_2 - D_2)}{dn} + Q'_{n2} \quad (42h)$$

where the dashed quantities are expressed in terms of products of first-order forced perturbations and are reported in Appendix A.

4.3. *Mixed mode*

At $O(\nu\epsilon^{\frac{1}{2}})$ mixed interactions give rise to $_{11}$ components satisfying the following differential system

$$L_{11}\begin{pmatrix} U_{11} \\ V_{11} \\ H_{11} \\ D_{11} \end{pmatrix} + \begin{pmatrix} 0 \\ 0 \\ 0 \\ -\dfrac{i\omega_c}{Q_0 \Phi_0}(F_0^2 H_{11} - D_{11}) \end{pmatrix} = \begin{pmatrix} b_1^{(11)} \\ b_2^{(11)} \\ b_3^{(11)} \\ b_4^{(11)} \end{pmatrix}, \quad (43a\text{–}d)$$

$$V_{11} = R(F_0^2 H_{11} - D_{11}) - Q'_{n11} = 0 \quad (n = \pm 1), \quad (43e, f)$$

where L_{11} is a differential operator obtained from L_1 by replacing λ_m with $(\lambda_m+\lambda_c)$ and the coefficients $b_j^{(11)}(n)$ read:

$$\begin{aligned} b_1^{(11)} &= -i(\lambda_m+\lambda_c)U_1 u_1 S_1-(U_{1,n}+1)v_1 C_1-\tfrac{1}{2}\pi V_1 v_1 C_1 \\ &\quad -\tfrac{1}{2}\pi k_1(2u_1+d_1)C_1-\beta_c C_0 T'_{s11} \\ &\quad -\beta_c C_0[D_1(2d_1-t_{s1})-T_{s1}d_1+n(t_{s1}-d_1)]S_1, \end{aligned} \tag{44a}$$

$$\begin{aligned} b_2^{(11)} &= -i\lambda_m V_1 u_1 S_1-i\lambda_c U_1 v_1 C_1-V_{1,n}v_1 C_1 \\ &\quad +\tfrac{1}{2}\pi V_1 v_1 S_1-k_1[-\pi v_1+i\lambda_c(2u_1+d_1)+2i\lambda_m u_1]S_1 \\ &\quad -n\tfrac{1}{2}\pi h_1 C_1+2u_1 S_1-\beta_c C_0[T'_{n11}+t_{n1}(n-D_1)C_1-T_{n1}d_1 S_1], \end{aligned} \tag{44b}$$

$$\begin{aligned} b_3^{(11)} &= -i(\lambda_m+\lambda_c)(D_1 u_1+U_1 d_1)S_1-(V_{1,n}S_1+\tfrac{1}{2}\pi V_1 C_1)d_1 \\ &\quad +[\tfrac{1}{2}\pi(D_1+n)S_1-(D_{1,n}+1)C_1]v_1, \end{aligned} \tag{44c}$$

$$b_4^{(11)} = -i(\lambda_m+\lambda_c)Q'_{s11}-Q'_{n11,n}+ni\lambda_c q_{s1}S_1-q_{n1}C_1. \tag{44d}$$

Moreover decompositions similar to (42*a–h*) have been employed for the $O(\nu\epsilon^{\frac{1}{2}})$ 1-1 components of bottom stresses and bed-load components as follows:

$$T_{s11} = s_1 U_{11}+s_2 D_{11}+T'_{s11}, \tag{45a}$$

$$T_{n11} = V_{11}+T'_{n11}, \tag{45b}$$

$$Q_{s11} = f_1 U_{11}+f_2 D_{11}+Q'_{s11}, \tag{45c}$$

$$Q_{n11} = V_{11}-R\frac{d(F_0^2 H_{11}-D_{11})}{dn}+Q'_{n11}, \tag{45d}$$

where the dashed quantities are again reported in Appendix A.

The differential problem for $_{11}$ components of the solution is obtained from (43*a–f*), (44*a–d*) and (45*a–d*) by replacing $(i\lambda_c, i\omega_c)$ with $(-i\lambda_c, -i\omega_c)$ and the coefficients of the $O(\epsilon^{\frac{1}{2}})$ fundamental free mode $(u_1, v_1, \ldots, q_{n1})$ with their complex conjugates.

The differential problems (35), (39), (43) and the one governing the $_{11}$ components have been solved both analytically (details of the solutions given in Appendix B) and numerically using a fourth-order Runge–Kutta scheme. Analytical and numerical solutions were found to agree up to the 7th significant figure.

$O(\epsilon^{\frac{3}{2}}, \nu^2\epsilon^{\frac{1}{2}})$

If we set

$$\nu = k_i \epsilon^{\frac{1}{2}} \tag{46}$$

with k_i an $O(1)$ parameter, the differential system obtained for the $O(\epsilon^{\frac{3}{2}})$ free fundamental mode reproduced by free interactions is also affected by $O(\nu^2\epsilon^{\frac{1}{2}})$ mixed interactions, as discussed above, through non-homogeneous terms which are proportional to $k_i^2 A(T)$. Under these conditions we find the following linear system for $(u_{11}, v_{11}, h_{11}, d_{11})$

$$L\begin{pmatrix} u_{11} \\ v_{11} \\ h_{11} \\ d_{11} \end{pmatrix}+\begin{pmatrix} 0 \\ 0 \\ 0 \\ -\dfrac{i\omega_c}{Q_0 \Phi_0}(F_0^2 h_{11}-d_{11}) \end{pmatrix}=\begin{pmatrix} A^2\bar{A}p_1+A(p_2+k_i^2 p_2^1) \\ A^2\bar{A}p_3+A(p_4+k_i^2 p_4^1) \\ A^2\bar{A}p_5+A(p_6+k_i^2 p_6^1) \\ A^2\bar{A}p_7+A(p_8+k_i^2 p_8^1)+p_9\dfrac{dA}{dT} \end{pmatrix}, \tag{47a–d}$$

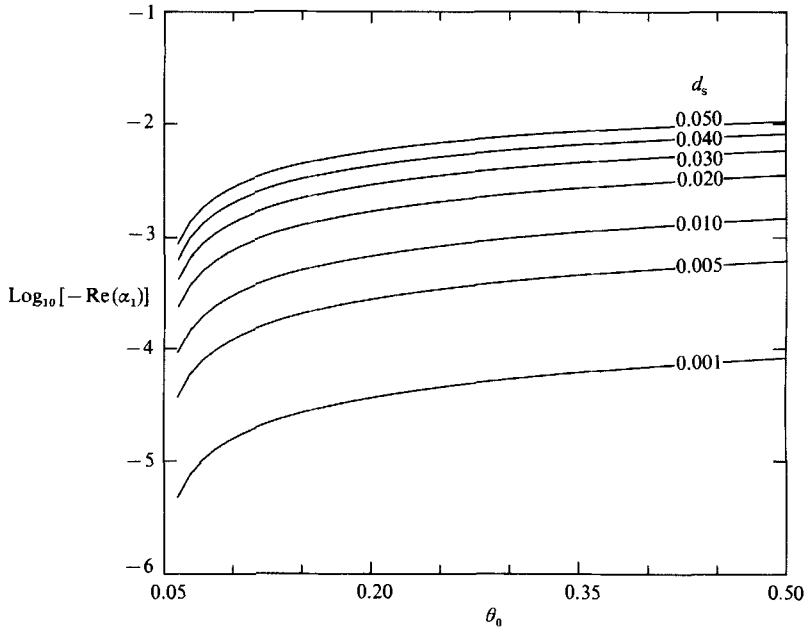

FIGURE 5. The real part of the coefficient α_1 of the amplitude equation (49) is plotted versus θ_0 for some values of the grain ratio d_s.

where L is the linear algebraic operator governing the fundamental free mode which is obtained from L_1 by replacing λ_m with λ_c, (d/dn) by $(-\frac{1}{2}\pi)$ everywhere but in a_{23} where (d/dn) is replaced by $(\frac{1}{2}\pi)$ and (d^2/dn^2) by $(-\frac{1}{4}\pi^2)$. The quantities p_{1-9} are determined by free interactions and are identical with those derived in CST (see equation (50)), whereas the quantities p_2^1, p_4^1, p_6^1, p_8^1 are lengthy algebraic expressions involving the first- and second-order free, forced and mixed components of the flow and bottom perturbation. They are given in detail in Appendix B.

For the system (47) solvability is ensured provided the following condition be satisfied:

$$\begin{vmatrix} a_{11} & a_{12} & a_{13} & A^2\bar{A}p_1 + A(p_2 + k_i^2 p_2^1) \\ a_{21} & a_{22} & a_{23} & A^2\bar{A}p_3 + A(p_4 + k_i^2 p_4^1) \\ a_{31} & a_{32} & a_{33} & A^2\bar{A}p_5 + A(p_6 + k_i^2 p_6^1) \\ a_{41} & a_{42} & a_{43} & A^2\bar{A}p_7 + A(p_8 + k_i^2 p_8^1) + p_9 \dfrac{dA}{dT} \end{vmatrix} = 0 \tag{48}$$

Equation (48) is readily found to reduce to the following nonlinear ordinary differential equation for the amplitude function $A(T)$:

$$\frac{dA}{dT} + (\alpha_1 + k_i^2 \alpha_{11}) A + \alpha_2 A^2 \bar{A} = 0, \tag{49}$$

where α_1 and α_2 are complex coefficients identical with those obtained in CST (see equation (52)) while α_{11} is the coefficient associated with the effect of mixed interactions analysed in the present contribution. Each of the above coefficients is a function of the unperturbed Shields stress θ_0 and of the grain ratio d_s. The coefficient α_{11} is also a function of the meander wavenumber λ_m. Plots for $\mathrm{Re}(\alpha_1)$ and $\mathrm{Re}(\alpha_2)$ are given in figures 5 and 6, while $\mathrm{Re}(\alpha_{11})$ is expressed below (see equation (50)) in

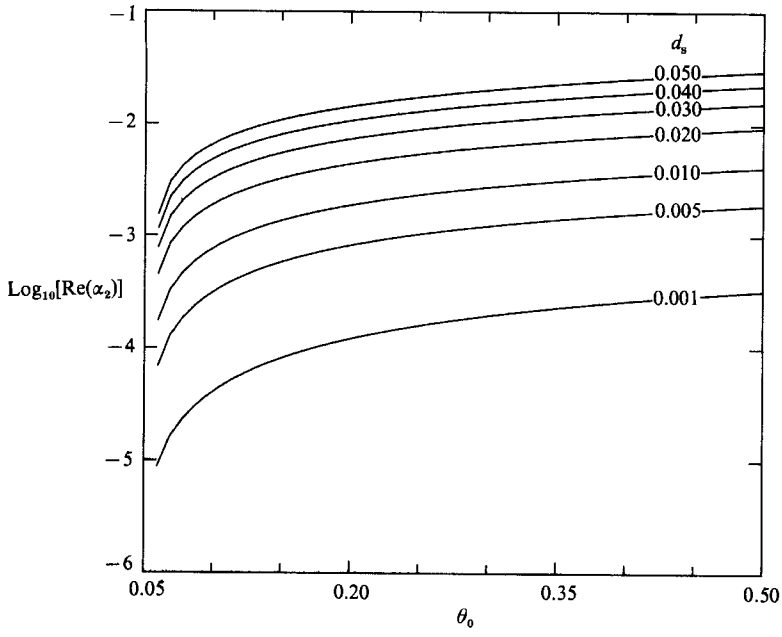

FIGURE 6. The real part of the coefficient α_2 of the amplitude equation (49) is plotted versus θ_0 for some values of the grain ratio d_s.

terms of the critical value of k_i for free bar suppression which is plotted in figure 9 for typical values of θ_0, d_s and λ_m/λ_c.

5. Critical curvature for free bar suppression

Equation (49) is of Landau–Stuart type and exhibits some important features.

Firstly as $k_i \to 0$ we recover the amplitude equation derived in CST for the straight channel case.

For finite k_i, equation (49) allows for supercritical equilibrium amplitude solutions as $T \to \infty$ provided $\mathrm{Re}\,(\alpha_1 + k_i^2 \alpha_{11})/\mathrm{Re}\,(\alpha_2)$ be negative. Thus curvature affects the existence of free bars: indeed in CST $\mathrm{Re}\,(\alpha_1)/\mathrm{Re}\,(\alpha_2)$ was always found to be negative whence, in order for curvature to tend to suppress alternate bars, we expect that $\mathrm{sgn}\,[\mathrm{Re}\,(\alpha_{11})] \neq \mathrm{sgn}\,[\mathrm{Re}\,(\alpha_1)]$. Under the latter conditions $\mathrm{Re}\,(\alpha_1 + k_i^2 \alpha_{11})$ changes sign for some critical value k_{c1} of k_i defined as

$$k_{c1} = \left(-\frac{\mathrm{Re}\,(\alpha_1)}{\mathrm{Re}\,(\alpha_{11})} \right)^{\frac{1}{2}}. \tag{50}$$

For values of λ_m/λ_c such that a critical value k_{c1} defined as in (50) exists the critical value ν_{c1} of the curvature ratio able to suppress free bars is given by the following relationship

$$\nu_{c1} = k_{c1} \left(\frac{\beta - \beta_c}{\beta_c} \right)^{\frac{1}{2}}. \tag{51}$$

Physically equation (51) simply states that the larger the amplitude of free bars the more sinuous the channel should be in order to suppress them. The dependence of ν_{c1} on β predicted by formula (51) is fairly strong but could not be detected by KM who designed their experiments such that β was held constant. Also notice that k_{c1} is in

general a function of the unperturbed Shields parameters θ_0, the grain roughness d_s and the meander wavenumber λ_m.

The second important feature of equation (49) concerns the behaviour of the speed of free bars as k_t increases. In fact, at equilibrium, we can write

$$A_e = |A_e| \exp(i\hat{\omega}T), \tag{52}$$

with

$$\hat{\omega} = \mathrm{Im}(\alpha_1) + k_t^2 \mathrm{Im}(\alpha_{11}) + |A_e|^2 \mathrm{Im}(\alpha_2), \tag{53}$$

whence the dimensionless wavespeed C_b of free bars is affected by curvature according to the following relationship:

$$C_b = \lambda_c(-\omega_c + \epsilon\hat{\omega}) = \lambda_c(\omega_1 + \nu^2\omega_2), \tag{54}$$

where the expressions for ω_1 and ω_2 are readily derived using (46), (53) and (54). Thus curvature will slow down or speed up the propagation of free bars depending on ω_2 being negative or positive. If the former condition is found to occur (54) allows us to define a second critical value of the curvature ratio ν_{c2} as the value of ν such that C_b vanishes. We find

$$\nu_{c2} = \left(-\frac{\omega_1}{\omega_2}\right)^{\frac{1}{2}} = \left(\frac{\omega_c - \epsilon[\mathrm{Im}(\alpha_1) + |A_e|^2 \mathrm{Im}(\alpha_2)]}{\mathrm{Im}(\alpha_{11})}\right)^{\frac{1}{2}}, \tag{55}$$

where ν_{c2} will again be a function of θ_0, d_s, λ_m and β.

Thus the following regimes appear to be possible:

(i) If $\nu_{c1} < \nu_{c2}$ free bars are damped and slowed down for $\nu < \nu_{c1}$ and are suppressed for $\nu > \nu_{c1}$.

(ii) If $\nu_{c1} > \nu_{c2}$:

free bars are damped, slowed down but migrate downstream for $\nu < \nu_{c2}$;

free bars are damped and migrate upstream (though possibly at a very low rate) for

$$\nu_{c2} < \nu < \nu_{c1};$$

free bars are suppressed for $\nu > \nu_{c1}$.

Let us then come to KM's experimental observations. Some quantitative comparison between our theoretical predictions of the critical values $k_{c1}\,(\equiv \nu_{c1}/\epsilon^{\frac{1}{2}})$ and $k_{c2}\,(\equiv \nu_{c2}/\epsilon^{\frac{1}{2}})$ and experimental data is pursued in figures 7(*a*) and 7(*b*) respectively.

Before commenting on the above comparison it is necessary to state the procedure employed to perform it. In the calculations, the values of θ_0, d_s and β given in KM for each experiment were used assuming the relative density of coal to be 1.5, the initial bottom configuration to be plane and finally evaluating ν_{c1} and ν_{c2} (given by (51) and (55) respectively) as functions of λ_m. The corresponding critical values α_{c1} and α_{c2} of the angle between straight segments of KM's channel were associated with ν_{c1} and ν_{c2} respectively using the relationships:

$$\nu = \tfrac{1}{4}\pi\lambda'_m \tan(\tfrac{1}{2}\alpha), \quad \lambda_m = \lambda'_m[1 - (\tfrac{1}{4}\pi \tan(\tfrac{1}{2}\alpha))^2 + O(\tan^2(\tfrac{1}{2}\alpha))], \tag{56a, b}$$

where λ'_m is the experimental KM's value of the dimensionless meander wavenumber in Cartesian coordinates. Notice that (56*a*) is obtained by modelling KM's sequence of straight segments by a sequence of meanders, the centreline of which is given in Cartesian coordinates by a sinusoid with maximum curvature and intrinsic wavenumber respectively equal to those characteristic of the equivalent 'sine generated curve' adopted in the theoretical model. However the sinusoidal model of

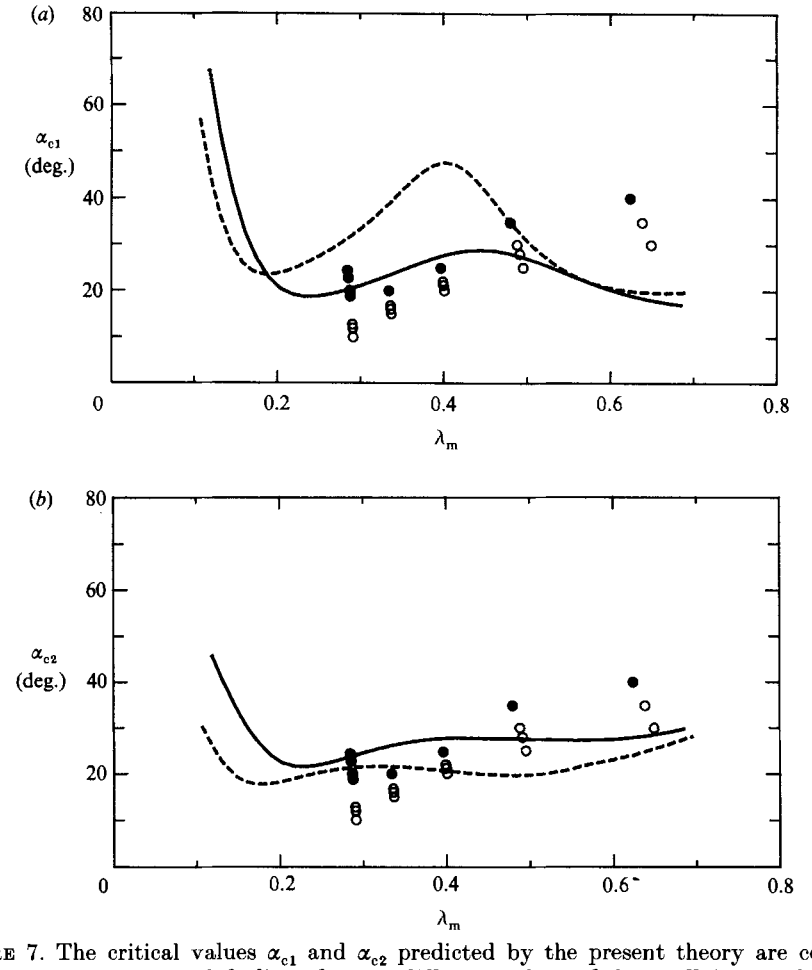

FIGURE 7. The critical values α_{c1} and α_{c2} predicted by the present theory are compared with KM's (1974) experimental findings for two different values of the coefficient r of equation (22). ——, $r = 0.5$; – – –, $r = 0.3$; ●, non-migrating; ○, migrating.

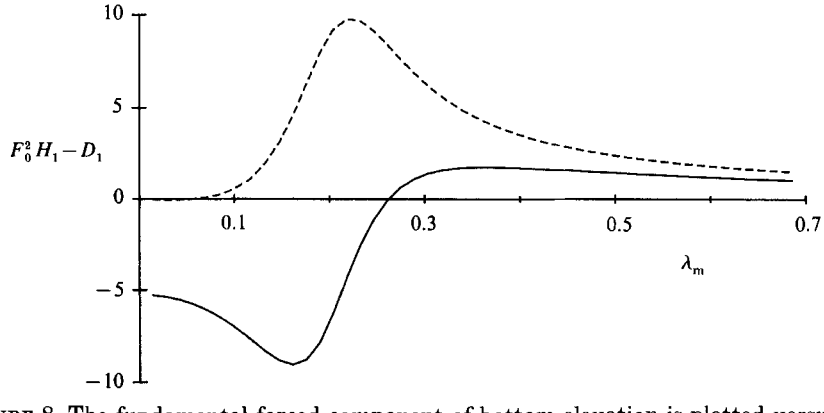

FIGURE 8. The fundamental forced component of bottom elevation is plotted versus the meander wavenumber λ_m showing that the resonant peak corresponds to maximum free bar suppression. Data as in KM's experiments. ——, real part; – – –, imaginary part.

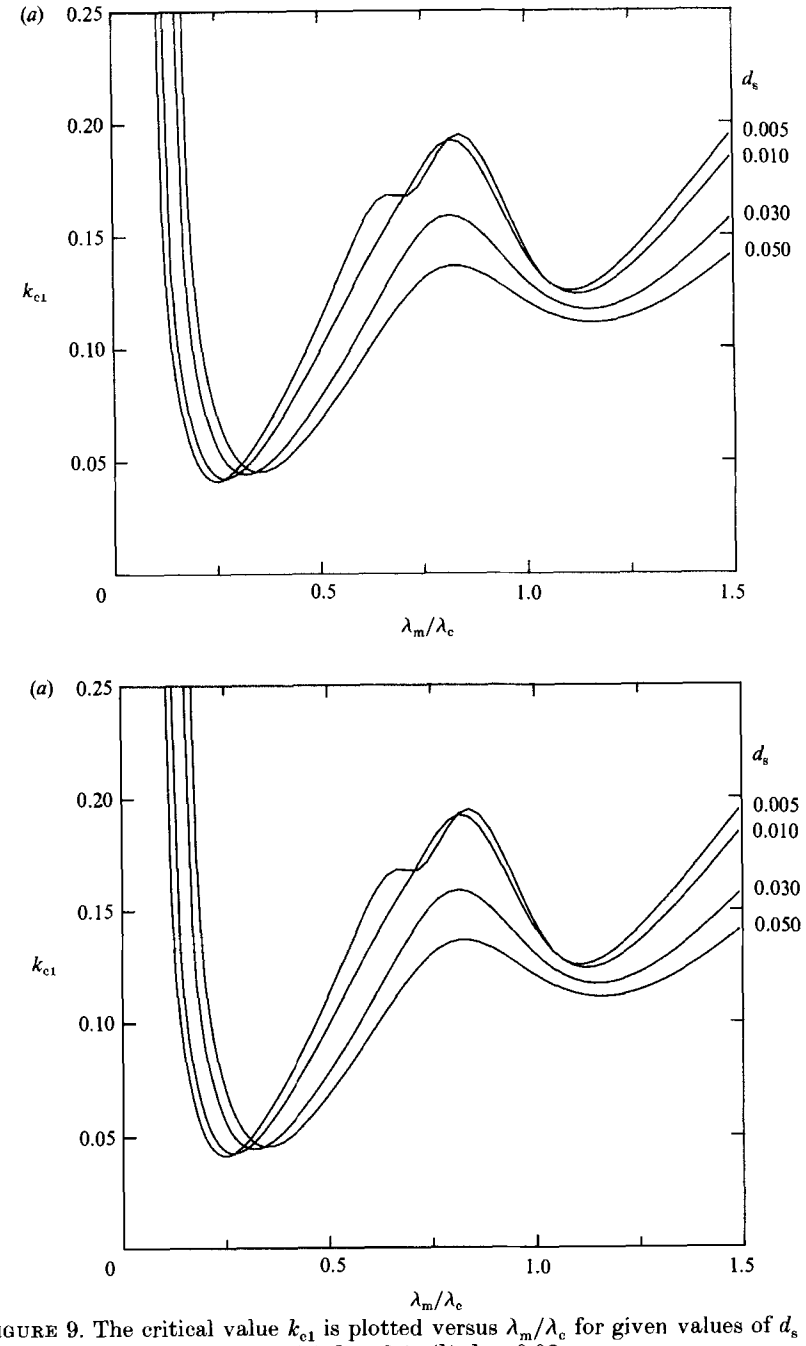

FIGURE 9. The critical value k_{c1} is plotted versus λ_m/λ_c for given values of d_s and θ_0: (a) $\theta_0 = 0.1$; (b) $d_s = 0.02$.

KM's configuration and the 'sine generated' model differ between each other by quantities $O[\tan^2(\frac{1}{2}\alpha)]$. Both of them are anyhow only approximate representations of KM's configuration.

Sensitivity of theoretical predictions to the choice of the empirical coefficient r of equation (22) is also shown in figure 7.

Various observations arise from figure 7. The signs of $\mathrm{Re}(\alpha_{11})$ and $\mathrm{Im}(\alpha_{11})$ are

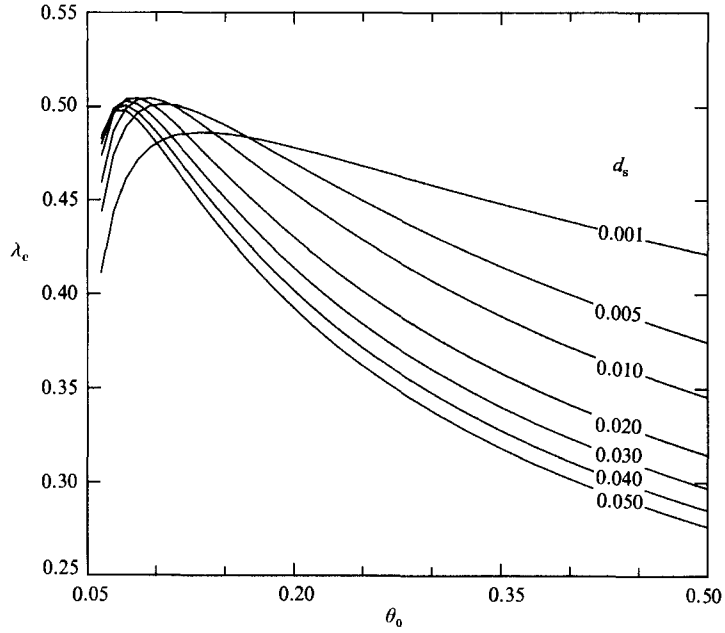

FIGURE 10. The critical bar wavenumber λ_c is plotted versus θ_0 for some values of the grain ratio d_s.

found to be such that critical values ν_{c1} and ν_{c2} exist in a wide range of values of λ_m/λ_c including those corresponding to KM's experiments. The distribution of α_{c1} and α_{c2} are very close to each other and both exhibit a trend which appears to be in fairly good agreement with experimental observations. The criterion employed by KM to define α_c was to ascertain 'whether an initially formed bar train could migrate more than one wavelength downstream'. However the boundary between the 'migrating' and 'non-migrating' regimes was unclear: 'It was sometimes observed that clearly visible bar fronts would be unable to migrate more than one wavelength downstream and would tend to vanish..., but that nevertheless the point of deepest scour along the bank would subsequently be subject to oscillations in elevation that would not fade in time.'

The precise mechanism operating at the transitional regime can only be ascertained through detailed experimental observations as KM themselves pointed out. However the agreement exhibited by figures 7(*a*) and 7(*b*) appears to strongly support the correctness of the physical ideas underlying the present investigation.

From figure 7 it appears that there are ranges of values of λ_m such that $\nu_{c2} < \nu_{c1}$. Thus it should be possible to perform an experiment in these ranges where bars migrating upstream should be observed. However we point out that this regime appears to be associated with fairly large values of α such that the perturbation expansion employed herein might only be qualitatively valid. Thus the actual existence of this regime needs to be verified experimentally or by means of strongly nonlinear (possibly numerical) analyses.

Figure 7 also shows that the curves $\alpha_{c1}(\lambda_m)$ and $\alpha_{c2}(\lambda_m)$ have a minimum. This feature is of great conceptual and practical interest. In fact figure 8, which shows the dependence of the fundamental forced component of bottom elevation as a function of λ_m, clearly suggests that the minimum values of α_{c1} and α_{c2} are attained within the resonant wavenumber range of BS. This was not unexpected: indeed close to

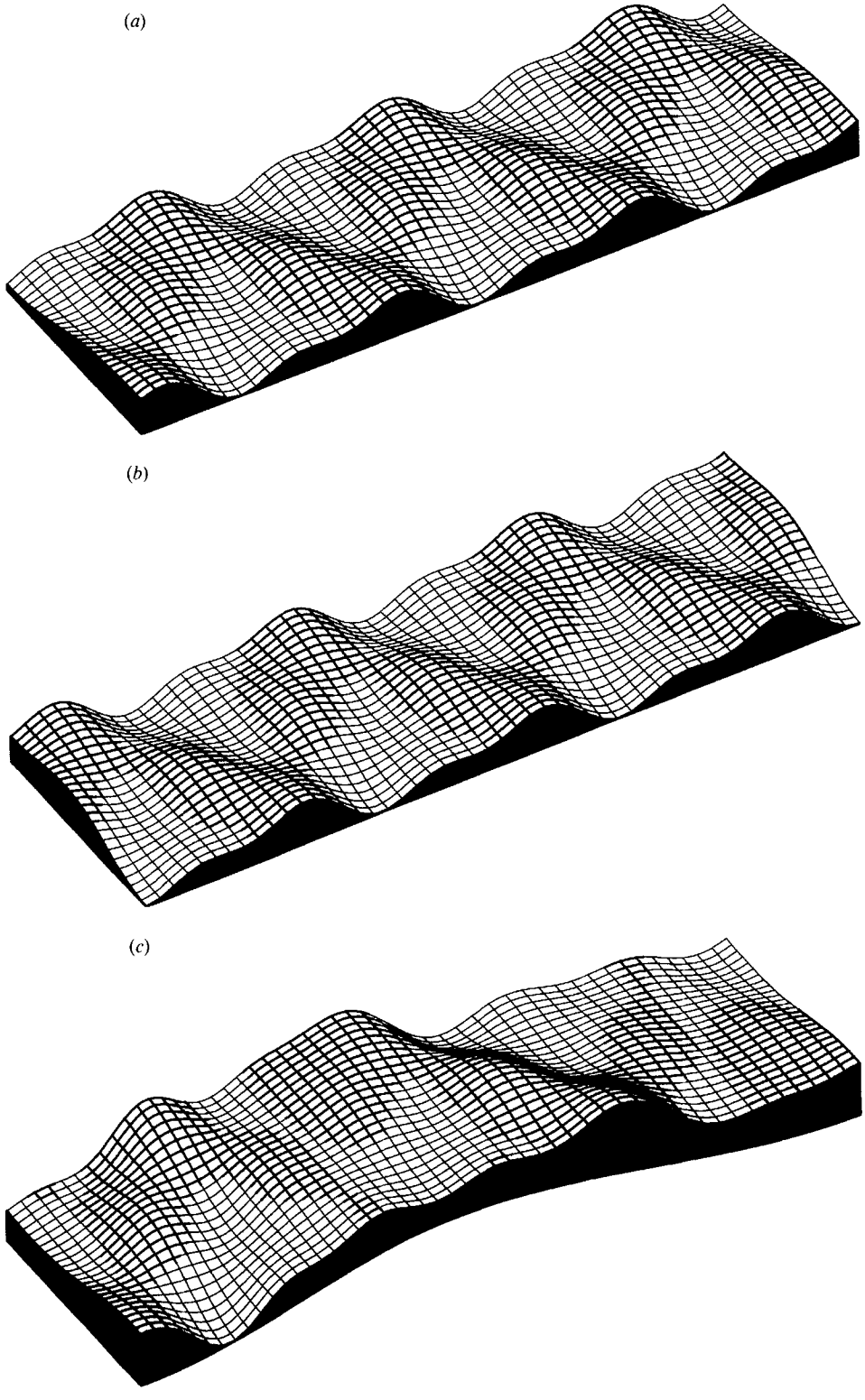

FIGURE 11 (*a–c*). For caption see facing page.

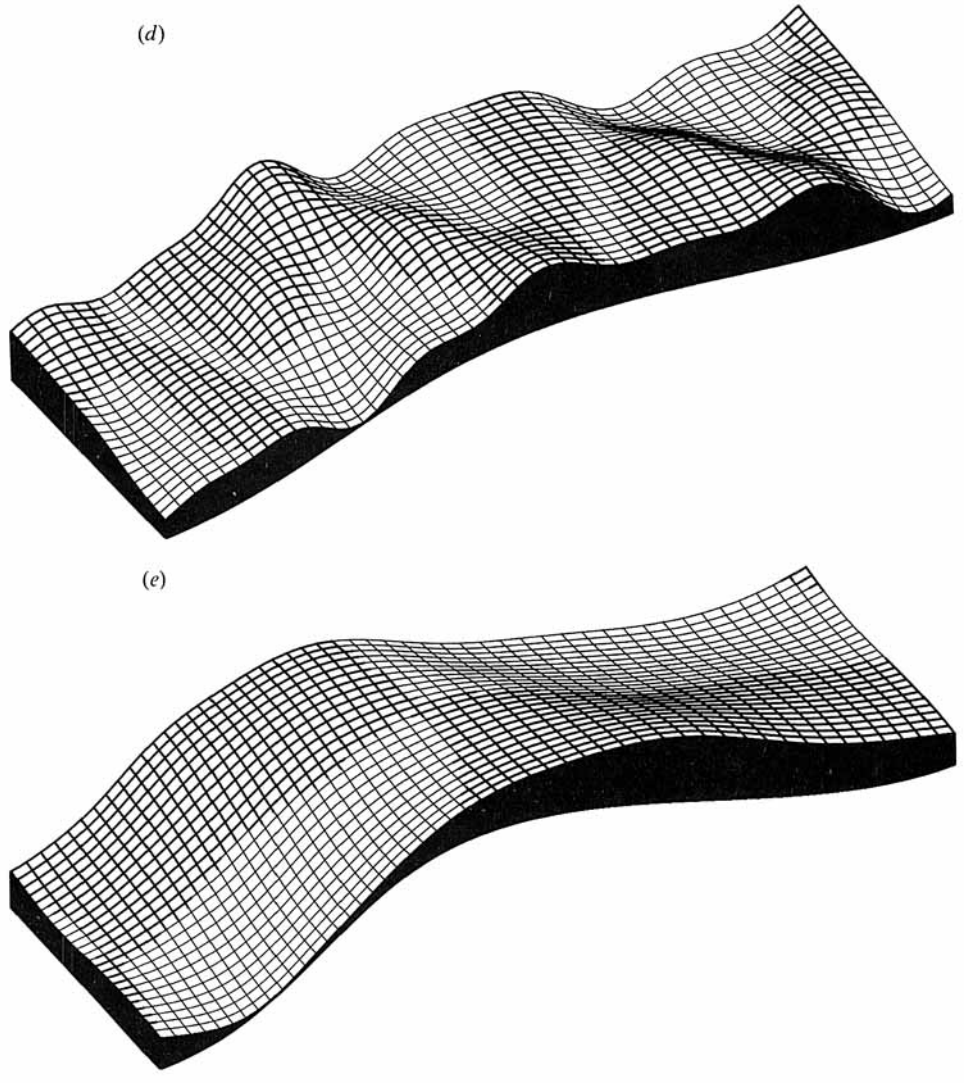

FIGURE 11. A three-dimensional view of bottom configuration is given showing pure free bars for $\nu = 0$ [(*a*) $\omega_c t = 0$; (*b*) $\omega_c t = \frac{4}{3}\pi$], free bars coexisting with forced bars for $\nu = \frac{1}{2}\nu_{c1}$ [(*c*) $\omega_c t = 0$; (*d*) $\omega_c t = \frac{4}{3}\pi$] and free bars suppression for $\nu = \nu_{c1}$ (*e*). $\beta = 20$, $\theta_0 = 0.1$, $d_s = 0.01$, $\lambda_m/\lambda_c = \frac{1}{3}$.

resonance the forced bar exhibits a peak which implies that lower sinuosities are sufficient to damp free bars. Practically this suggests that, when a channel is artificially corrected the formation of free (migrating) bars might be prevented by giving the channel a relatively small sinuosity and choosing the wavenumber within the resonant range. There is obviously a price to pay for free bar suppression: the amplitude of forced bars is relatively large, with obvious implications regarding the use and management of the channel. However in the absence of free bars, under steady flow conditions, forced bars are steady, which is favourable for channel control.

Incidentally KM's results also exhibit a minimum for a value of the wavenumber close to that theoretically predicted: this might be taken as an indirect demonstration that resonance is experimentally observed.

The last noticeable feature of figure 7 is the behaviour of α_{c1} and α_{c2} as $\lambda_m \to 0$. It appears that free bars are enhanced by curvature if meanders are long enough. This result conforms to the field observations of Kinoshita (1961) who noticed that in tortuous bends several alternate bars may be superimposed over a primary point bar.

The above findings are confirmed for different values of θ_0 and d_s as shown in figure 9 where k_{c1} is plotted as a function of the ratio of the meander wavenumber λ_m to the bar wavenumber λ_c. The latter, along with formula (51), figure 6 of CST plotting the critical width ratio for free bar formation $\beta_c(\theta_0; d_s)$ and figure 10 plotting the critical bar wavenumber $\lambda_c(\theta_0; d_s)$, allows one to determine the critical value of the curvature ratio for free bar suppression provided θ_0 and d_s are given such that the unperturbed bottom configuration be plane. Figure 9 also shows the existence of a second minimum in the curve $k_{c1}(\lambda_m/\lambda_c)$ which occurs for values of λ_m/λ_c close to 1. This feature is vaguely reminiscent of a spatially synchronous Mathieu-type response, though the migrating character of part of the perturbation further complicates here the characteristics of the process. The second minimum disappears as θ_0 and/or d_s increase. This explains why it was not revealed by KM's experiments.

Finally, figure 11 gives a pictorial three-dimensional description of the process of interaction between free and forced bars in meandering channels as it emerges from the present theory. These pictures allows one to follow the progressive slowing down and suppression of free bars as the curvature ratio of the channel ν increases from 0 up to ν_{c1}, for given values of β, θ_0, d_s and λ_m. Figures 11 (*a*) and 11 (*b*) show free bars migrating in a straight channel ($\nu = 0$) at $t = 0$ and $t = \frac{4}{3}\pi/\omega_c$ respectively: the wavespeed of bars may be estimated by comparing the two plots. When $0 < \nu < \nu_{c1}$ migrating free bars and steady forced bars may coexist and the amplitude and wavespeed of free bars decrease with respect to the straight case: this is shown in figures 11 (*c*)–11 (*d*) where $\nu = \frac{1}{2}\nu_{c1}$ and the same time interval between the two plots as in figures 11 (*a*) and 11 (*b*) is used. Finally figure 11 (*e*) shows the steady bed topography which appears when free migrating bars are suppressed ($\nu = \nu_{c1}$).

6. Conclusions

The theoretical framework built in the present contribution appears to draw a picture of the process of free–forced bar interactions which is consistent with various experimental and field observations.

Meander development is described in figure 9 by curves starting from the horizontal axis at some value of the ratio λ_m/λ_c (typically 0.3–0.4) and characterized by values of the latter ratio progressively decreasing as the intrinsic meander wavelength and the curvature ratio increase. It follows that, in the course of meander development, our theory predicts coexistence of free and forced bars for relatively low values of ν (as indicated by KM's and Gottlieb's (1976) observations), free bar suppression when $\nu(\lambda_m)$ exceeds $\nu_{c1}(\lambda_m)$ (in accordance with KM's results), reappearance of free bars when λ_m has become small enough for $\nu(\lambda_m)$ to be again smaller than $\nu_{c1}(\lambda_m)$ (in agreement with Kinoshita's (1961) field observations of 'tortuous' meanders).

Results have been presented only for the case when the unperturbed configuration is plane. The present theory is perfectly equipped to deal with the dune case if the presence of dunes is simply accounted for in terms of its effect on the friction coefficient and the bed load function. However, dunes are likely to interact with secondary flow induced by bars so as to affect the dynamics of transverse sediment

transport in a manner which has never been thoroughly analysed. Further experimental and theoretical work is needed.

Other features which may play a role in the process investigated in the present contribution are the effect of transport in suspension, grain sorting, entrance and wall effects, unsteadiness.

An extension of the present theory to account for strongly nonlinear effects ($\beta \gg \beta_c$, $\nu \sim O(1)$) appears to be feasible though it is likely to require a fairly heavy numerical approach. As has already been pointed out, such an extension does not seem to be necessary for forced bars as suppression of free bars appears to occur for fairly low values of ν. In order to model strongly nonlinear free bars it does not seem to be appropriate to extend the present weakly nonlinear perturbation technique. Rather it might be possible to formulate a still two-dimensional model able to fit oblique bottom discontinuities to represent the sharp bar fronts occurring in reality.

Finally the perturbation expansion employed herein breaks down for values of β and λ_m close to the resonant peaks where the forced response can no longer be represented by a straightforward expansion in integer powers of ν. Overcoming this limitation would require that a nonlinear theory of resonance be preliminarily formulated.

This work was supported by MPI-Project of National Relevance 'Fenomeni di Trasporto solido'. Preliminary versions of the present results were presented at Euromech 215 (S. Margherita Ligure, Genoa, September 1987) and at the joint US–Japan final meeting on River Meandering (Kauai Island, October 1987).

Appendix A

We report the expressions derived for second-order components of $\tau_s/C_0, \tau_n/C_0$, $Q_s/\Phi_0, Q_n/\Phi_0$ in terms of products of first-order quantities.

$O(\nu^2)$

$$T'_{s0} = (1-C_T)^{-1}[-3U_1\bar{U}_1+\tfrac{1}{2}C_{TT}T_{s1}\bar{T}_{s1}+\bar{T}_{s1}(2U_1+C_{TD}D_1) + \tfrac{1}{2}C_{DD}D_1\bar{D}_1+\tfrac{1}{2}(V_1+\bar{V}_1+C_T T_{n1}\bar{T}_{n1})]+\text{c.c.}, \quad (A\,1a)$$

$$T'_{n0} = [\bar{V}_1(T_{s1}-U_1)+\bar{k}_4 T_{s1}]+\text{c.c.}, \quad (A\,1b)$$

$$Q'_{s0} = \{[\Phi_{TD}D_1\bar{T}_{s1}+\tfrac{1}{2}\Phi_{DD}D_1\bar{D}_1+\tfrac{1}{2}\Phi_{TT}T_{s1}\bar{T}_{s1}+\tfrac{1}{2}(\Phi_T T_{n1}\bar{T}_{n1}-Q_{n1}\bar{Q}_{n1}) - \frac{\lambda_m^2}{2\beta_c^2}(F_0^2H_1-D_1)(F_0^2\bar{H}_1-\bar{D}_1)]+\text{c.c.}\}+\Phi_T T'_{s0}, \quad (A\,1c)$$

$$Q'_{n0} = [-U_1\bar{V}_1+\tfrac{1}{2}R\bar{T}_{s1}(F_0^2H_1-D_1)_{,n}+Q_{s1}\bar{Q}_{n1}]+\text{c.c.}, \quad (A\,1d)$$

$$T'_{s2} = (1-C_T)^{-1}[-3U_1^2+\tfrac{1}{2}C_{TT}T_{s1}^2+T_{s1}(2U_1+C_{TD}D_1)+\tfrac{1}{2}C_{DD}D_1^2+\tfrac{1}{2}(V_1^2+C_T T_{n1}^2)], \quad (A\,2a)$$

$$T'_{n2} = V_1(T_{s1}-U_1)+k_4 T_{s1}, \quad (A\,2b)$$

$$Q'_{s2} = \Phi_T T'_{s2}+\Phi_{TD}D_1T_{s1}+\tfrac{1}{2}\Phi_{DD}D_1^2+\tfrac{1}{2}\Phi_{TT}T_{s1}^2+\tfrac{1}{2}(\Phi_T T_{n1}^2-Q_{n1}^2)+\frac{\lambda_m^2}{2\beta_c^2}(F_0^2H_1-D_1)^2, \quad (A\,2c)$$

$$Q'_{n2} = -U_1V_1+\tfrac{1}{2}RT_{s1}(F_0^2H_1-D_1)_{,n}+Q_{s1}Q_{n1}. \quad (A\,2d)$$

$O(\nu\epsilon^{\frac{1}{2}})$

$$T'_{s11} = (1-C_T)^{-1}\{S_1[-6U_1 u_1 + C_{TT} T_{s1} t_{s1} + C_{DD} D_1 d_1 + C_{TD}(T_{s1} d_1 + D_1 t_{s1}) + 2T_{s1} u_1 + 2U_1 t_{s1}] + C_1[V_1 v_1 + C_T T_{n1} t_{n1}]\}, \quad (A\,3a)$$

$$T'_{n11} = S_1[V_1(t_{s1} - u_1) + k_4 t_{s1}] + C_1 v_1(T_{s1} - U_1), \quad (A\,3b)$$

$$Q'_{s11} = \Phi_T T'_{s11} + S_1[\Phi_{TT} T_{s1} t_{s1} + \Phi_{DD} D_1 d_1 + \Phi_{TD}(D_1 t_{s1} + T_{s1} d_1) + \frac{\lambda_c \lambda_m}{\beta_c^2}(F_0^2 H_1 - D_1)(F_0^2 h_1 - d_1)] + C_1(\Phi_T T_{n1} t_{n1} - Q_{n1} q_{n1}), \quad (A\,3c)$$

$$Q'_{n11} = S_1[\tfrac{1}{2}R(F_0^2 H_1 - D_1)_{,n} t_{s1} + Q_{n1} q_{s1} - V_1 u_1] + C_1[\tfrac{1}{4}R\pi T_{s1}(F_0^2 h_1 - d_1) + Q_{s1} q_{n1} - U_1 v_1]. \quad (A\,3d)$$

REFERENCES

Blondeaux, P. & Seminara, G. 1985 A unified bar-bend theory of river meanders. *J. Fluid Mech.* **157**, 449–470.

Blondeaux, P. & Seminara, G. 1988 Corrigendum on 'A unified bar-bend theory of river meanders.' *J. Fluid Mech.* **193**, 599.

Bray, D. I. 1979 Estimating average velocity in gravel bed rivers. *J. Hydraul. Div. ASCE* **105** (HY9), 1103–1122.

Callander, R. A. 1969 Instability and river channels. *J. Fluid Mech.* **36**, 465–480.

Chien, N. 1954 The present status of research on sediment transport. *J. Hydraul. Div. ASCE*, **80**.

Colombini, M., Seminara, G. & Tubino, M. 1987 Finite amplitude alternate bars. *J. Fluid Mech.* **181**, 213–232.

Engelund, F. 1974 Flow and bed topography in channel bends. *J. Hydraul. Div. ASCE* **100** (HY11), 1631–1648.

Engelund, F. 1981 The motion of sediment particles on an inclined bed. *Tech. Univ. Denmark ISVA Prog. Rep.* **53**, 15–20.

Engelund, F. & Hansen, E. 1967 A monograph on sediment transport in alluvial streams. Copenhagen: Danish Technical Press.

Gottlieb, L. 1976 Three-dimensional flow pattern and bed topography in meandering channels. *Tech. Univ. Denmark ISVA Series*, paper 11.

Ikeda, S. 1982 Lateral bedload transport on side slopes. *J. Hydraul. Engng ASCE* **108**, 1369–1373.

Ikeda, S., Parker, G. & Sawai, K. 1981 Bend theory of river meanders. Part 1. Linear development. *J. Fluid Mech.* **112**, 363–377.

Jaeggi, M. 1984 Formation and effects of alternate bars. *J. Hydraul. Engng ASCE* **110**, 142–156.

Johannesson, H. & Parker, G. 1989 Linear theory of river meanders. In *River Meandering* (ed. S. Ikeda & G. Parker), *AGU Water Resources Monograph* 12, pp. 181–213.

Kalkwijk, J. P. Th. & Vriend, H. J. de 1980 Computation of the flow in shallow river bends. *J. Hydraul. Res.* **18** (4), 327–342.

Kikkawa, H., Ikeda, S. & Kitagawa, A. 1976 Flow and bed topography in curved open channels. *J. Hydraul. Div. ASCE* **102** (HY9), 1326–1342.

Kinoshita, R. 1961 Investigation of channel deformation in Ishikari River. Rep. Bureau of Resources, Dept. Science & Technology, Japan, pp. 1–174.

Kinoshita, R. & Miwa, H. 1974 River channel formation which prevents downstream translation of transverse bars. *Shinsabo* **94**, 12–17 (in Japanese).

Olesen, K. W. 1983 Alternate bars and meandering of alluvial rivers. Commun. Hydraul. Delft University of Technology, Rep. 7–83.

Parker, G. 1984 Discussion of: 'Lateral bed load transport on side slopes' by S. Ikeda. *J. Hydraul. Engng ASCE* **110**, 197–199.

Parker, G. & Andrews, E. D. 1985 Sorting of bed load sediment by flow in meander bends, *Water Resources Res.* **21** (9), 1361–1373.

PARKER, G. & PETERSON, A. W. 1980 Bar resistance of gravel-bed streams. *J. Hydraul. Div. ASCE* **106** (HY10), 1559–1575.

SEMINARA, G. & TUBINO, M. 1985 Further results on the effect of transport in suspension on flow in weakly meandering channels. Colloquium on 'The Dynamics of Alluvial Rivers', Genova.

SEMINARA, G. & TUBINO, M. 1989 Alternate bars and meandering: free, forced and mixed interactions. In *River Meandering* (ed. S. Ikeda & G. Parker), *AGU Water Resources Monograph* 12, pp. 267–320.

SHEN, H. W. 1962 Development of bed roughness in alluvial channels. *J. Hydraul. Div. ASCE* **88** (HY3), 45–58.

VRIEND, H. J. DE 1981 Steady flow in shallow channel bends. Commun. Hydraul. Delft University of Technology.